ENGINEERED *IN VITRO* BREAST CANCER MODELS SHOW PHENOTYPIC DIFFERENTIATION CHARACTERISTICS OF EARLY *VS.* LATE-STAGE DISEASE

by

Harini Venkata Krishnan

Bachelor of Technology, Institute of Chemical Technology, 2014.

Submitted to the Graduate Faculty of

School of Pharmacy in partial fulfillment

of the requirements for the degree of

Master of Science

University of Pittsburgh

2016

UNIVERSITY OF PITTSBURGH

School of Pharmacy

This thesis was presented

by

Harini Venkata Krishnan

It was defended on

July 27, 2016

and approved by

Dr. Shilpa Sant, Assistant Professor, School of Pharmacy

Dr. Paul Johnston, Associate Professor, School of Pharmacy

Dr. Robert Gibbs, Professor, School of Pharmacy

Thesis Director Advisor: Dr. Shilpa Sant, Assistant Professor, School of Pharmacy

Engineered *In Vitro* Breast Cancer Models Show Phenotypic Differentiation Characteristics of Early *vs.* Late-Stage Disease

Harini Venkata Krishnan, B.Tech

University of Pittsburgh, 2016

Cancer drug discovery and development is challenged by poor prediction of drug responses in *in vitro* disease models. Results from clinical trials suggest that just 5% of drugs tested are successful in patients. Currently used disease models such as two-dimensional (2D) cell monolayers and *in vivo* animal models fail to recapitulate the human tumor microenvironment. Further, disease progression from the non-invasive to metastatic stage needs models that can recapitulate each stage. Hence, there is an unmet need to develop three-dimensional (3D) models that capture natural tumor progression for better understanding of disease biology as well as screening of drug regimens acting on different disease stages.

In this work, we have characterized 3D breast microtumors ranging from 150 to 600 μm diameters using non-invasive T47D cells with precise control over physicochemical microenvironmental factors. In this study, we test the hypothesis that the size-controlled microtumors will exhibit differential biochemical features and drug response arising from unique molecular signatures created by variable tumor microenvironments. To test this hypothesis, we studied the physicochemical features such as hypoxia, reactive oxygen species, metabolic activity, and cell cycle status. Additionally, the expression of key regulators of growth/proliferation pathways in breast cancer progression such as estrogen receptor alpha (ER-α) and growth factor receptor/s was studied and efficacy of clinically used inhibitors such as 4-hydroxytamoxifen (4-OHT) was evaluated.

The results indicated that large T47D microtumors (600 μm) exhibited traits of clinically advanced tumors such as collective cell migration, mesenchymal marker upregulation, loss of

ER-α and endocrine resistance in contrast to the small microtumors (150 μm). Thus, the engineered *in vitro* models could successfully recapitulate phenotypic differentiation characteristics of early *vs.* late disease stage in the same non-invasive T47D cells just by precisely controlling the microtumor size, which further regulated the tumor microenvironmental factors. The large microtumors (600 μm) were found to resemble features of advanced stage breast cancer whereas the small microtumors (150 μm) recapitulated features of early stage breast cancer. Hence, such disease stage-specific microtumor models could help in the evaluation of crucial mechanisms in breast tumor progression correlated to tumor size and in the screening of therapeutic candidate/s.

Keywords: 3D cell culture, stage specific model, breast cancer progression

TABLE OF CONTENTS

LIST OF FIGURES

ACKNOWLEDGMENTS

I would like to acknowledge the School of Pharmacy, University of Pittsburgh for granting me the opportunity to pursue my graduate studies. I express sincere gratitude to my advisor, Dr. Shilpa Sant for guidance, constant support and patience throughout my studies. I would like to thank Dr. Vinayak Sant for his valuable feedback and encouragement. I am thankful to Dr. Maggie Folan and other faculty from School of Pharmacy for their guidance. I would like to acknowledge Dr. Manjulata Singh for the training in technical skills, mentorship and continual support during my studies.

I express gratitude to our collaborators, Dr. Steffi Oesterreich and her lab member, Dr. Sreeja Sreekumar, for assistance with western blot experiments. I would like to thank Dr. Robert Gibbs for access to confocal microscope. I would like to acknowledge Dr. Jan Beumer and Brian Kiesel for running the mass spectrometry of our samples. Acknowledgments are due to Dr. Ipsita Banerjee and her student Sharlee Mahoney, for access and help with flow cytometer.

I would like to thank all members of Sant Lab - Yingfei Xue, Akhil Patel, Yohann Pitale, Lavanya Kondiparthi, Supraja Ranganathan, Sricharani Balmuri, Prithvirajan Durairajan, Piyusha Sane, and alumni for their unflinching assistance, feedback and support throughout my studies. I would like to thank members from Dr. Wen Xie, Dr. Paul Johnston, Dr. Robert Gibbs and Dr. Sean Xie's lab for their generous help in experiments. I am thankful to Lori Altenbaugh for her kind help in administrative support.

Finally, I express deep gratitude to my parents, grandparents, my sister Manasa and friends whose constant support and care was essential in completion of my studies.

1. INTRODUCTION

3D cell culture models in cancer

Development of anti-cancer drugs has been a challenging issue for the medical and pharmaceutical fraternity. Cell culture studies are an integral part of drug discovery and development as well as cancer biology studies. Traditionally, cells have been grown as monolayers on flat surfaces like petri plates or tissue culture flasks. However, it was realized that tissues and organs *in vivo* possessed 3D structure that enabled cell-cell and cell-matrix interactions [2]. Thus, over the past two decades many researchers have tried designing 3D models to reliably resemble the native tissue environment [3]. The two main categories of 3D models for cancer discovery are listed below.

Spheroids

Spheroids are multicellular aggregates that mimic natural tumors. They consist of only one or more kind of cells (tumor cell, stem cell, fibroblasts, etc.) isolated from specific cell lines. Alternatively, they can be fragments of the cancerous tissue/organ. They are spontaneously formed when cell-cell interactions overweigh cellular interactions with other entities (ECM, hormones, endogenous ligands, etc.) [4].

The multicellular architecture of spheroids mimics solid tumors *in vivo*. They are typically formed in the size range of 100 to 200 microns in diameter [5]. 3D multicellular structure causes diffusion limitation for oxygen and nutrients resulting in differential zones of proliferating and non-proliferating cells inside the spheroid. This simulates the metabolic profile generally observed naturally during tumor progression *in vivo* [6].

Spheroids can be produced by many techniques either in a suspension or gel embedded system. The hanging drop technique is one of the oldest methods which consist of cells inside a droplet of culture medium suspended on the underside of a culture dish [7]. Other methods for generating spheroids include growing cells in non-adherent surfaces such as agar, basement membrane, etc. The non-adherent surface enables cells to move towards each other and form aggregates [5].

Alternative methods for spheroid generation involve continuous agitation of culture suspension inside spinning flasks and NASA rotary vessels that avoid cells from settling down [8]. These methods are preferred for large scale production. However, these agitation techniques require special equipment and produce non-uniform spheroids. This non-uniformity makes spheroid production less reproducible. Advances in microfabrication technology have led to the formation of spheroids inside microwell arrays [9]. While some groups use photolithography to imprint micrometer size wells on non-adhesive polymer surfaces, others have scaled up this technique to 96 well plate [10].

Additionally, spheroids have been embedded inside gels made up of collagen, Matrigel and polyethylene glycol (PEG) [8]. Such encapsulation provides for interactions between cells and ECM. Further, some researchers have developed heterogeneous spheroids in these gels by co-culturing two types of cells like fibroblasts and epithelial cells [11].

Scaffolds

Tissue engineering has led to the development of novel materials for several biological and therapeutic applications. Scaffold based 3D models involve culturing cells on or inside a naturally or synthetically derived polymers [12]. Natural polymers like collagen or agarose and

biocompatible synthetic polymers such as Poly lactic-co-glycolic acid, PEG have been used popularly to engineer 3D scaffolds with tuneable properties [12].

Fabrication techniques like electrospinning can control ECM-mimicking fibrous structure of these scaffolds at nanoscale. This helps to establish contacts and guide cells seeded similar to *in vivo* conditions. Electrospinning parameters such as voltage, polymer solution flow rate, viscosity of solution, etc. can be optimized to produce scaffold of interest. Besides this, small amount of polymers are required in this process making it highly cost effective [13].

Differences in 3D *vs* 2D culture

Studies have suggested that cells cultured in 2D are different from 3D with respect to morphology, growth kinetics and genotypic/phenotypic traits [14]. Cells grown on 2D have a different morphology as compared to 3D cultures. Gurski et al [15] observed that prostate cancer cells seeded on a plastic layer had a spread-out morphology whereas they acquired round clustered morphology when cultured in 3D hyaluronic acid hydrogels. Cells in 3D culture possess growth kinetics similar to *in vivo* tumors [16]. Akin to this feature, metabolic activity of cells cultured in 3D is markedly different from 2D cells as they have more barriers for diffusion of endogenous substrates [17]. Breast cancer cells seeded on 3D chitosan scaffold were found to produce more glucose and lactate compared to monolayers [18]. Many studies have demonstrated that 3D culture affects genotypic and phenotypic characteristics of cells [19, 20]. The genotype of cells cultured as 2D is very different from patient derived tumor samples however it matches with cells cultured as 3D [21]. Seminal work in this field highlights that the features demonstrated by 3D models such as clustered morphology, growth kinetics, metabolic profile and drug resistance resemble those of *in vivo* tumors [22-24].

Applications in anti-cancer drug screening

Further, cells cultured as 3D respond to anti-cancer drugs in a different manner compared to 2D [25]. Therefore, anti-cancer drug/s screening was performed in soft agar assays, a gold standard, for several years [26]. Cells grow in soft agar assays in an anchorage independent manner and this growth is strongly correlated to tumorigenicity in animal models. But this assay is usually slow, labor-intensive and inconsistent because of subjective definitions of colonies [27].

Using a novel hanging drop technique in 384 well plate, spheroids were formed robustly to handle high throughput screening [28]. When anticancer drug sensitivity was tested, cells in the 3D model showed significantly more viability compared to 2D culture upon treatment with 5-Fluorouracil (an antimetabolite). In contrast, treatment with Tirapazamine (hypoxia activated drug) resulted in higher cytotoxicity in 3D due to presence of hypoxia.

Human oral cancer cells seeded in engineered 3D poly lactide-co-glycolide (PLG) scaffolds resulted in decreased sensitivity to PI3-kinase inhibitor LY294002 in contrast to 2D cells suggesting that drug efficacy is dependent upon microenvironmental factors such porous structure of 3D PLG scaffolds [21]. The importance of specific microenvironment in this study was further enhanced by the lack of drug resistance exhibited in a control 3D Matrigel model.

On similar lines, Iwase and co-workers developed a 3D model consisting of hepatic cancer sheet sandwiched by two collagen sheets in order to mimic natural tissue organization found *in vivo* i.e. cancer cells surrounded by stroma [29]. Upon treatment with doxorubicin it was observed that 3D culture was resistant as compared to 2D. Some groups recently have developed 3D culture models with a dynamic setup to enable a more accurate prediction of chemotherapeutics administered intravenously *in vivo.* Multicellular tumor spheroids of breast cancer (MCF-7) were generated and cultured in a microfluidic device using photolithography that simulated conditions *in vivo* [30]. Treatment by doxorubicin in static as well as dynamic

conditions resulted in decreased drug sensitivity of 3D spheroids compared to monolayer cultures.

Human epidermal growth factor receptor 2 (HER2) positive subtype breast cancer cells in laminin rich 3D ECM gels acquired a switch in HER2 downstream signalling pathways from PI3K-AKT to RAS-MAPK [31]. This switch was not observed in 2D cells. In addition, 3D culture of AU565 and SKBR3 cells showed opposing sensitivities to Transtuzumab (HER2 targeted antibody), even though they possess same levels of HER2 family proteins.

Doxorubicin (DOX) micelles delivered to multicellular tumor spheroids of breast cancer cells could be visualized through fluorescence microscopy depicting accumulation of DOX micelles on the surface of spheroids between cells [30]. This spatial information about DOX micelles can help us to understand the drug penetration and carrier effects. Similarly, intracellular trafficking of histamine-functionalized copolymer DOX micelles was performed in spheroids of breast cancer cells. Compared to 2D, the co-localization of DOX in lysosomes was much lesser in spheroids suggesting difficulty to penetrate inside the cellular aggregates [32]. In another study, polymersomes loaded with DOX and paclitaxel required longer exposure time for eliciting cytotoxic response in 3D spheroid model of head and neck cancer as compared to 2D [33].

Taken together, it is clear that 3D culture models offer cues resembling the native tumor microenvironment that shape the response of drug/s making it significantly different from 2D. In addition, since most 3D models confer drug resistance arising from diffusional barriers compared to 2D, they can be used to eliminate or optimize drug candidates that depict good sensitivity in 2D cytotoxicity assays. This will help in reducing costs and saving time for drug discovery and development process.

Tumor microenvironment in cancer progression

Complex mechanisms and inter-related signalling pathways shape the onset and progression of cancer. The microenvironment strongly influences the homeostasis and development of normal and malignant tissues [34]. In all tissues, multiple types of cells co-exist surrounded by the ECM and endogenous chemicals (chemokines, growth factors, etc.). The interplay amongst these components and cells result in their specific function. In a similar fashion, tumor tissues are also regulated by their physiological milieu. Neoplastic cells in solid tumors reside along with stromal cells (epithelial cells, fibroblasts, dendritic cells, macrophages, vascular endothelial cells) in ECM. During tumor development, diffusional gradients in oxygen and nutrients, ECM density, activation of immune cells, induction of growth factors influence disease progression. Invasion and metastasis, the final stages of any cancer, also occur due to several survival mechanisms adopted by aggressive tumors in communication with neighbouring environment [14, 22].

Breast cancer and its hallmarks during tumor progression

Breast cancer is a clinically heterogeneous disease that leads to 10–15% of patients developing aggressive tumors/ distant metastases within a few years of primary tumor detection [35]. This progression of breast cancer is typically categorized by the ‘stage’ of the disease such as non-invasive (stages 0-2) to invasive (stages 3-4) stage. Interestingly, as per the National Cancer Institute’s database, the five-year survival rates drop from 100% in stage 0 to 22% in stage 4.

Clinically, the breast tumor progression involves dynamic organization of epithelial cells with stromal cells as represented in **Figure 1 (upper panel)**. The primary cancer cells and cellular as well as acellular components (ECM) of tumor microenvironment evolve with tumor progression from primary to invasive and metastatic stage **Figure 1 (lower panel)**. This change is caused by altered physicochemical features in the tumor microenvironment such as hypoxia, acidic pH, levels of reactive oxygen species/ metabolic markers, matrix stiffness and porosity [36]. Further, the development of advanced breast cancer from ductal carcinoma in situ exhibits certain hallmarks that characterize tumor progression. Epithelial to mesenchymal transition (EMT), collective cell migration and angiogenesis are the most common hallmarks that are described in the following section [1].

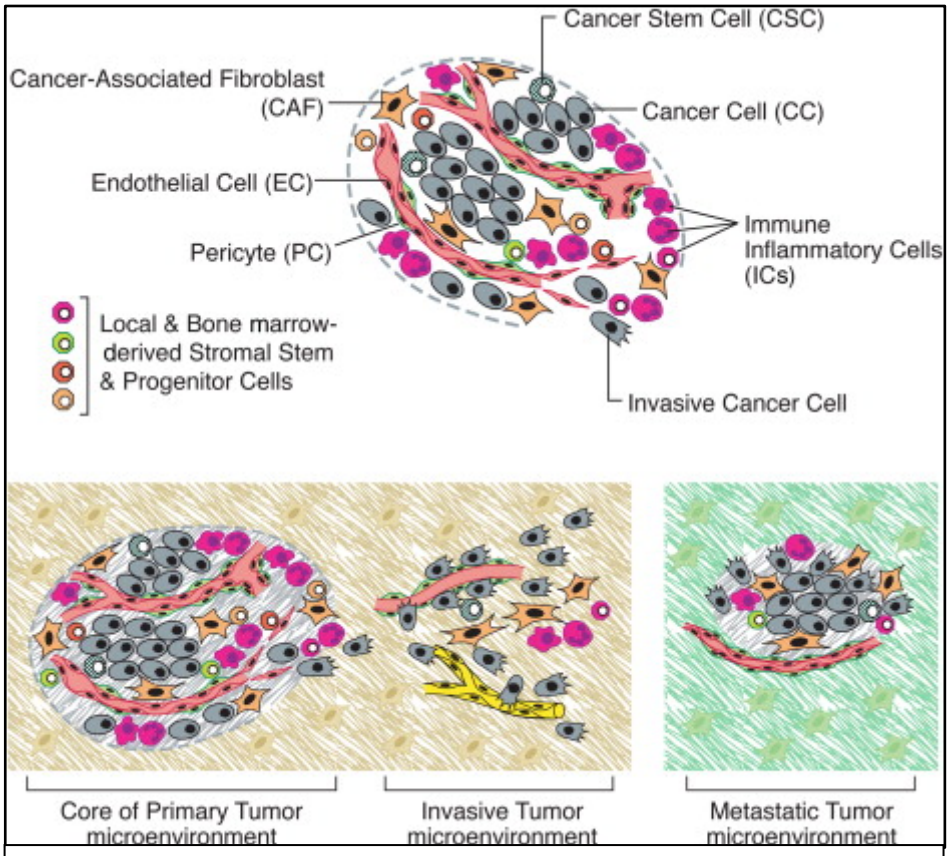

Figure 1: Schematic of breast cancer progression [1].

Epithelial to mesenchymal transition

Epithelial cancer cells acquire ability to invade, disseminate from primary tumors and metastasize to other organs. This change in their programming is known as epithelial to

mesenchymal transition (EMT). As seen from Figure 1, the morphology of epithelial cancer cell changes to mesenchymal i.e. invasive cancer cell type during this process. At the gene level, EMT is characterized by increased expression of transcriptional factors such as Snail, Slug and Twist, as well as mesenchymal markers like vimentin and fibronectin [1]. Additionally, some studies report loss of E-cadherin that promotes cell-cell adhesion making these cancer cells disseminate from the primary tumor site. Moreover, a “cadherin switch” is observed with gain of N-cadherin, which enables transition to the mesenchymal phenotype [37]. Cumulatively, this classical reprogramming of epithelial cells to mesenchymal type has been investigated in many types of solid tumors making it an accepted hallmark of cancer progression.

Collective cell migration

During the EMT, cancer cells can detach from the primary core tumor either as a single cell or as a collective cohort of cells [38]. This cohort of cells retains cell-cell adherent junction proteins. These cells interact dynamically with the neighbouring environment and generate physical forces or traction to provide motility to primary tumor.

Angiogenesis

Most of the solid tumors are avascular, and can grow up to a size of 1–2 cubic millimetres [39]. Beyond this size, the oxygen and nutrient supply to primary tumor reduces greatly. This generates a region of hypoxia in these tumors. In such scenario, these tumor cells fulfil their need by recruiting surrounding host blood vessels that can subsequently infiltrate the tumor mass, allowing for propagation of tumor and potential for metastatic spread of tumor mass *via* blood. This process is called angiogenesis. The induction of angiogenesis is found to be associated with upregulation of growth factors such as basic fibroblast growth factor and vascular endothelial growth factors (Vegf).

Changes pertaining to ER + subtype breast cancer progression

ER-alpha has been established as a prognostic factor for breast cancer patients with ER+ subtype [40]. Mechanistic studies on survival pathways in ER+ breast tumor progression indicate that early stage tumors are majorly driven by ER signalling pathway while advanced stage tumors lose dependence on this pathway due to genetic or post-translational loss of ER [41]. ER+ breast cancers are effectively managed by endocrine therapy during an initial period of five years. However, around 30% of patients develop endocrine resistance and metastases in the long term [42].

Clinical literature suggests dependence of advanced stage ER+ tumors on growth factor receptors as alternative survival pathway [42]. Therefore, drugs targeting receptor tyrosine kinase such as tyrosine kinase inhibitors and antibodies are employed to combat endocrine resistance during the later stages of the disease [43]. For illustration, Transtuzumab, a human epidermal growth factor receptor (HER2) antibody, was used to treat patients in clinical trials that had acquired endocrine resistance. This study indicated that complete pathological response in patients improved after administration of HER2 targeted agents [44].

Additionally, many therapies incorporate use of chemotherapeutics such as doxorubicin (acting on all actively proliferating cells) along with targeted inhibitors to improve efficacy and prolong lifespan of advanced stage patients [44].

Importance and unmet need for stage-specific *in vitro* tumor models

The dynamic progression of breast cancer is presently investigated using 2D tumor cell line cultures and *in vivo* animal models. In 2D cell culture models, researchers often use non-invasive cell lines like MCF7/T47D to mimic early stage and invasive cell lines like MDA-MB-231 to capture the late stage of the disease [45]. These cell lines are derived from patients

belonging to early and late metastatic stage, respectively. However, such use of cell lines with different molecular signatures cannot reliably depict progression of tumor taking place within a patient with over time. Other studies involve manipulations in the same cell line by exposure to artificial conditions like hypoxic chambers or silencing/overexpression of genes to mimic tumor progression [46]. These studies also have limitations because artificial manipulation of cellular machinery can dysregulate other mechanisms influencing tumor progression [47].

Mouse xenograft models may be better *in vivo* tools, as they possess a more complex physiological system. However, the target tissue expression, metabolic processes and immune system are significantly different from humans resulting in varied toxicity/efficacy profiles of potential drug candidates [48, 49]. Alternatively, breast tumor biopsies and tissue microarrays can be useful in identifying metastatic and aggressive tumor phenotypes but lack of availability of biologically matched tumor samples limits progress in the field [50].

Thus, there is an unmet need to develop *in vitro* models that can mimic the natural tumor progression in real time without use of artificial conditions. Such *in vitro* models would be of great value to screen drugs that act on various molecular targets activated at different stages during tumor progression. Besides establishing the safety and efficacy of potential drug candidates, such models could also provide the right platform to study major molecular pathways that regulate tumor growth pertaining to specific stages in tumor progression. This could allow researchers to develop therapies that can combat the disease in a more effective manner.

Therefore, we rationally designed stage-specific models to mimic breast cancer progression by controlling the size of microtumors. Tumor size is a widely used prognostic marker of stage-wise breast cancer progression [51]. Hence, we developed uniform, size-controlled microtumors where size was controlled by seeding cells on hydrogel microdevices with uniform size microwells fabricated using with micropatterning technique [52]. As demonstrated in our

previous work [53], these novel size-controlled microtumor models recapitulated physiological milieu of solid tumors such as development of hypoxia, induction of metabolic stress and central necrotic zone of cells surrounded by peripheral proliferating cells.

In the current work, we hypothesized that microtumor size-dependent physicochemical changes in the tumor microenvironment will lead to progression of non-invasive breast cancer microtumors (T47D) to aggressive advanced stage microtumors defined by acquisition of mesenchymal phenotype and migratory behaviour. We predicted that 600 µm microtumors (referred to as large microtumors hereafter) would resemble advanced stage breast cancer characteristics such as biochemical features and response to drug/s due to similarity with pathological microenvironment of advanced stage clinical samples, achieved by virtue of increased microtumor size. Similarly, 150 µm microtumor (referred to as small microtumors henceforth) will mimic attributes of early stage breast cancer.

Our data suggests that large microtumors depict the late stage of the disease while small ones show the traits of early stage tumors. Additionally, clinically observed hallmarks of late stage tumors such as loss of ER-α and endocrine resistance were observed in large microtumors but not in the small ones. In addition, mechanisms for observed drug resistance were explored. Cumulatively, these results indicate that the stage specificity and high clinical relevance of size-controlled microtumor models can be effectively exploited for discovery of breast cancer therapeutics.

2. MATERIALS AND METHODS

2.1 Cell culture

The T47D breast cancer cell line was received from Prof. Steffi Oesterreich's lab (Magee Women's Research Institute, UPCI, Pittsburgh). All the cell culture supplies and media were obtained from Corning and Mediatech, respectively unless specified. T47D cells were cultured in T75 flasks that contained DMEM medium supplemented with 10% FBS (Hyclone, Utah, USA) and 1% penicillin-streptomycin. T47D cell flasks were cultured in a humidified incubator maintained at 37 °C and 5% CO_2. Prior to seeding into hydrogel microwell arrays, cells were cultured to achieve 40-60% confluence.

2.2 Materials and reagents

All chemicals were purchased from Sigma Aldrich (St. Louis, MO) unless specified. The antibodies (anti ER-alpha F-10 sc8002, anti-EGFR 1005 sc03G) were procured from Santa Cruz Biotechnology (California, USA). The antibody anti-beta actin (MA5-15739-D680) was purchased from Thermo Scientific Inc. (Rockford, USA) while anti-phospho EGFR (Tyr 845) [2231S], anti-Akt [9272S], anti-phospho Akt (Ser 473) [4060S], anti-ERK 1/2 [9102S], anti-phospho ERK 1/2 (Thr 204/Tyr 202) [4370P] were obtained from Cell Signaling Technology (Danvers, MA, USA). All secondary antibodies (Dylight 690, 800, Alexa Fluor 488, 594) were secured from Thermo Scientific Inc. (Rockford, USA). 4-hydroxytamoxifen was purchased from Sigma Aldrich (St. Louis, MO). Ruthenium-tris (4, 7-diphenyl-1, 10-phenanthroline) dichloride

(Ru-dpp) was acquired from Santa Cruz Biotechnology, (California, USA). 2', 7' – dichlorodihydrofluorescin diacetate (DCHFDA) was procured from Cayman Chemicals (Michigan, USA). Propidium iodide was obtained from Sigma Aldrich (St. Louis, MO) and RNAse I solution from Thermo Scientific Inc. (Rockford, USA).

2.3 Three dimensional (3D) microtumor fabrication

Microtumors of breast cancer cells (T47D) were fabricated as detailed in the previous work [53]. Briefly, using cylindrical polydimethylsiloxane (PDMS) posts of 150 and 600 µm (diameter and height), wells were imprinted on polyethylene glycol dimethacrylate (PEGDMA) substrate containing 1% photoinitiator (Irgacure, BASF, USA) and 20% PEGDMA in a photocrosslinking technique. After crosslinking of hydrogel and formation of wells, the devices were sterilized in 70% isopropanol under UV for 45 min. Following this process, devices were washed three times with DPBS to remove isopropanol and observed under microscope for any imperfections/air bubbles. T47D cells (2x 10^4 cells/µL) were added to each device with 1 cm x 1cm dimensions in a 24 well plate and allowed to settle for 30 min. This was followed by another round of cell addition. After this step, excess cells were washed away carefully by DPBS, and media was added to the wells containing devices in culture plates and kept in the incubator.

2.4 Reactive oxygen species and intra-tumoral oxygen measurement

These experiments were performed to analyse whether microtumor size affects physicochemical features of solid tumors such as reactive oxygen species and hypoxia. T47D

microtumors were cultured as described above for 6 days by replenishing wells with fresh media each day after removal of 50% media. For reactive oxygen species detection, 10 µM DCHFDA was added to the microtumors and cultured for 3 hours in an incubator. After a wash with PBS, microtumors were imaged using a confocal microscope (Olympus Fluoview, Olympus). To determine intra-tumoral oxygen availability, fluorescence of Ru-dpp, (excitation, λmax 455 nm, emission λmax 613 nm), was used. Ru-dpp fluorescence is quenched in presence of oxygen thus enabling us to determine regions of hypoxia. Microtumors were incubated in 10^{-4} µM Ru-dpp solution for 3 hours and images of Ru-dpp stained microtumors were acquired on a confocal microscope (Olympus Fluoview, Olympus). Background fluorescence was accounted by imaging culture media containing Ru-dpp without microtumors.

2.5 Metabolic activity measurement in microtumors

In order to study effect of microtumor size on growth of microtumors, metabolic activity of small and large microtumors was assessed using the standard alamarBlue® assay [54]. This assay is based on the principle that the viable cells reduce resazurin to resorufin. Resazurin, the main component of alamarBlue® reagent, is a non-toxic, cell permeable compound that is blue in color and virtually non-fluorescent. Upon entering cells, resazurin is reduced to resorufin, a compound that is red in color and highly fluorescent. Viable cells continuously convert resazurin to resorufin, increasing the overall fluorescence. The conversion measured in terms of fluorescence of the dye is proportional to viability/metabolic activity of the samples. This assay has been optimized and used in previous studies from the lab [55].

The T47D microtumors were cultured as mentioned before in a 24 well plate. On the required day (1, 3 or 6), 10% alamarBlue® solution (Thermo Scientific, Rockford, USA) was freshly

prepared in growth media (DMEM+10%FBS+1%Penicillin/Streptomycin). The media from all wells was discarded and 600 µL of 10% alamarBlue® solution was added to each well containing microtumors. After three hours of incubation (37°C), the plate was removed and the solution was gently mixed using a micropipette. The supernatant from wells was transferred to a 96 well plate and the culture plate was replenished with fresh media. The 96 well plate was read for fluorescence at excitation 530 nm and emission 590 nm by a microplate reader (H1 Synergy, Biotek Instruments, Winooski, VT, USA). After required days of culture, the 24 well plate was removed from incubator and alamarBlue® assay was performed similarly. The percentage (%) growth for each device containing microtumors was calculated as per the formula [(Average of fluorescence values at Day # (1, 3 or 6)/ Average of fluorescence values at Day 1)] x100.

2.6 Cell cycle analysis in microtumors

We further investigated effect of various physicochemical changes in the tumor microenvironment (hypoxia, ROS) on cell cycle progression in small (150 µm) *vs.* large (600 µm) microtumors. Small and large microtumors were cultured as outlined above. The media was changed every day. After required days in culture (1, 3 or 6), microtumors were harvested gently and collected in microcentrifuge tubes and pelleted using centrifugation for 3 min at 1200 RPM. The pellet was washed with PBS and trypsinized for 7-10 min. After quenching the cell suspension with media, cells were pelleted using centrifugation. The pellet was suspended in 500 µL of cold PBS. The cell suspension was added dropwise to 500 µL of cold absolute ethanol. The sample was observed for clumping and any visible clumps were removed using tweezers. The microcentrifuge tubes sealed with parafilm were stored at 4 °C overnight. After this fixing process, cells were washed with cold PBS and centrifuged at 400 RPM for 10 min.

The pellet was resuspended in 300 µL of 50 µg/mL propidium iodide solution (containing 100 µg/mL RNAse I solution). The tubes were vortexed briefly and incubated at 37 °C for 30 min. The data was acquired on a flow cytometer (BD Accuri C6, BD Biosciences, New Jersey, USA). For all the groups, total number of events recorded in the FL2-A vs FL2-H channel was 15000. The histograms were analysed using ModFit LT software (Verity Software House, Maine, USA).

2.7 RNA isolation and q-PCR analysis

In order to study the changes in the expression of genes involved in various pathways (*e.g*. epithelial-mesenchymal transformation, EMT) in microtumors, mRNA expression was analysed by quantitative PCR. RNA isolation was performed using GeneJET RNA purification kit (Thermo Scientific, Lithuania, EU) as per the manufacturer's instructions. Frozen microtumor samples were lysed in the commercially supplied lysis buffer with addition of β-mercaptoethanol by vortexing for 5 min, ethanol addition and incubation at room temperature for 5 min. The mixture was passed through GeneJet purification columns and washed multiple times with kit buffers at 12000 RPM for 1 min. Total RNA adsorbed onto the columns was eluted by using nuclease free water provided with the kit. RNA concentration was measured using Nanodrop and RNA quality was determined by absorbance ratio at 260/280 nm. Estrogen receptor alpha mRNA expression was estimated by qRT-PCR after generating cDNA using 500 ng mRNA and iTaq Universal SYBR Green RT-PCR kit (BioRad Laboratories Inc., USA). Briefly, reaction mixture containing 2 µL cDNA, 5 µL of 2X SYBR green master mix and respective primers (0.2 µM) was amplified in triplicates. For estrogen receptor, the forward primer sequence is 5' AACCGAGATGATGTAGCCAG 3' while reverse primer sequence is 5' CAGGAACCAGGGAAAATGTG 3'.

Other primer sequences were as described in previous work [53]. The amplification protocol used was 40 cycles of denaturation for 15 sec at 95 °C, annealing for 30 sec at 55 °C and extension for 30 sec at 72 °C (7500 Fast Real-Time PCR System, Applied Biosystems, California, USA). mRNA expression was calculated using $2^{-\Delta\Delta Ct}$ method [56] and depicted as the mean ± SEM as fold change compared to the controls (day 1 samples).

2.8 Protein extraction and western blotting

The goal of this experiment was to evaluate changes in the expression of proteins of interest as a function of time in culture and microtumor size. Frozen microtumors were homogenized in RIPA buffer containing Tris (50 mM, pH 7.4), NaCl (150 mM), sodium deoxycholate (0.5%), nonyl phenoxypolyethoxylethanol-40 (1%), phenylmethylsulfonyl fluoride (0.05 mM), protease inhibitor cocktail for mammalian tissue extract and phosphatase inhibitor cocktail (Sigma-Aldrich Inc., Milwaukee, USA). Total protein content was quantified by Coomassie Plus (Bradford) Assay kit (Thermo Scientific, Rockford, USA).

Fifty microgram protein samples were separated by 8-10% SDS-PAGE and transferred onto 0.45 µm PVDF membrane (Thermo Scientific, Rockford, USA). The PVDF membrane was blocked in Odyssey Blocking Buffer (PBS based), (LiCor Biosciences, Nebraska, USA) for 2 h at room temperature. Further, blots were probed with primary antibodies (1:1000), by incubating overnight at 4 °C. Later on, the membrane was washed thrice with PBS containing 0.1% Tween-20 (PBST) and incubated with respective fluorescently conjugated secondary antibodies for 2 h at room temperature on a rocking platform. The membranes were developed by scanning in Odyssey Infrared Imaging System (LI-COR® Biosciences, Lincoln, USA) and coloured images

were converted to grayscale by using Odyssey 3.0 software. Densitometry analysis of blots was done by ImageJ Software (National Institute of Health, USA).

2.9 Immunofluorescence studies

The immunofluorescence studies were used to probe differences in intra-tumoral and subcellular localization of proteins as a function of microtumor size. Harvested microtumors were fixed with 4% paraformaldehyde for 30 min at room temperature, washed with PBST to remove residual PFA and again fixed with 95% methanol on ice for 15 min. Permeabilization with 0.1% Triton X-100 was done for 1.5 hours followed by blocking with 3% BSA to avoid non-specific binding. Microtumors were placed on depression slides and incubated with primary antibody (1:100) overnight at 4 °C in a humidified chamber along with a negative control (without primary antibody). After washing three times with PBST, microtumors were incubated with fluorescently labelled secondary antibodies for 1 h at room temperature. Nuclei were stained by incubating with Hoechst (1:300) at 4 °C overnight. After two washes with PBS, glycerol was added to stained microtumors and kept at 4 °C until confocal imaging. Images were acquired on confocal microscope (Olympus Fluoview, Olympus) as a z-stack containing a series of 5-µm slices using 10X (lower magnification) or 40X (higher magnification) objectives with or without zoom factor. The images are presented as 2D projection of maximum intensity.

2.10. Measurement of 4-Hydroxytamoxifen (4-OHT) response in microtumors

As mentioned in the introduction, several studies have reported differential drug response in 2D *vs.* 3D cultures [5, 14, 25, 30]. With our ability to control precisely the microtumor size, we sought to determine if the drug response would be affected by microtumor size and possible mechanisms for such differential response. As the cell line used throughout this study was T47D, ER+ cell line, selective estrogen receptor modulator (SERM), 4-OHT was selected as a drug, which also remains the mainstay in the clinical management of ER+ patients. The T47D cells were seeded in hydrogel devices (1 cm x 1 cm) kept in 24 well plates and cultured for three days as described previously. For drug treatment, 10 mM 4-OHT (stock solution) was solubilized in DMSO. Further, 50 µM 4-OHT in growth media was prepared and stored away from light. On day 3, media from wells was removed and metabolic activity was assessed by adding 600 µL of 10% alamarBlue® solution (Thermo Scientific, Rockford, USA) freshly prepared in growth media. Only 10% alamarBlue® solution was used as a blank sample and the plate was kept in incubator (37°C). After three hours of incubation, the plate was removed and the solution was gently mixed using a micropipette. Seven devices per condition (untreated, and treated for both 150 µm and 600 µm) were used. Supernatant (150 µL x3) from each well was assayed for fluorescence intensity using excitation 530 nm and emission 590 nm by a microplate reader (H1 Synergy, Biotek Instruments, Winooski, VT, USA). After removal of the remaining alamarBlue® solution, 600 µL of drug solution was added to the wells (treatment groups) while fresh media with equal volume of DMSO was added to wells (control/vehicle groups). The culture plate was replaced back into the incubator for a period of three days. On day 6, the microtumors were analysed for metabolic activity again using alamarBlue® assay. % Growth for microtumors in each device was calculated with vehicle treated control taken as 100% growth as per the formula:

% Growth = [(Average of fluorescence values at Day 6)/ Average of fluorescence values at Day 3)] x100.

2.11 4-OHT quantification in microtumors by mass spectrometry

We further quantified the amount of 4-OHT in the treated microtumors. The harvested microtumors were washed with DPBS, pelleted and potassium chloride -Tris HCl buffer was added. This mixture was sonicated for 15 seconds and incubated on ice for 2 hours. The mixture was analysed by LC-MS/MS method.

2.11.1 Analytical

An LC-MS/MS method was used to quantitate 4-OHT (Sigma-Aldrich, St. Louis, MO) in microtumor lysate using [D_6]-4-hydroxytamoxifen (Toronto Research Chemicals, North York, Ontario, Canada) as an internal standard.

The HPLC method consisted of an Agilent 1100 autosampler and Agilent 1100 binary pump (Agilent Technologies, Palo Alto, CA) using a Synergi Polar-RP 80A (4 µm particle size, 2 mm x 100 mm) column at ambient temperature. Mobile phase solvent A was 0.1% formic acid (*v/v)* in methanol, and mobile phase solvent B was 0.1% formic acid (*v/v)* in water. Isocratic mobile phase conditions were used with 78% mobile phase A pumped at 0.3 mL/min for the entire duration of the 5 min run time. Retention time was 1.5 min.

A Waters Quattro Micro (Milford, MA) mass spectrometer was used in positive-ion MRM mode (4.0 kV capillary voltage, 40 V cone voltage, 22 V collision voltage) to monitor *m/z* 388.0>72 for 4-hydroxytamoxifen and *m/z* 394.0>78.0 for [D_6]-4-hydroxytamoxifen.

2.11.2 Sample preparation

Standards (10, 30, 100, 300, 1000, 3000, 5000 and 10000 ng/mL) were prepared in a 50/50 mixture of potassium chloride lysis buffer and human plasma (Lampire Biological Laboratories Inc., Pipersville, PA). For microtumor samples, 50 µL of microtumor lysate sample was

combined with 50 µL of blank plasma to match the 100 µL calibrator sample matrix and volume. Resulting microtumor lysate sample concentrations were corrected for the dilution after analysis. Internal standard solution (10 µL of 1 µg/mL) was added to each tube prior to addition of sample. A volume of 300 µL of ice cold methanol was then added and the samples vortexed for 1 min using a Vortex Genie-2 (Scientific Products, Bohemia, NY). Samples were then centrifuged at 12,500 x g for 3 min and 100 µL of the resulting supernatant was transferred to an autosampler vial. The sample injection volume was 5 µL.

2.12 Statistical analysis

Results are depicted as mean ± SEM (standard error of mean) from three independent experiments each with triplicates or more. A one-way or two-way analysis of variance (ANOVA) followed by a Tukey's multiple comparison-test was used to compare control and test groups. A *p*-value less than 0.05 was considered significant. Graph Pad Prism (V6.0) was used to perform the statistical analysis.

3. RESULTS AND DISCUSSION

3.1 Microtumor size affects physicochemical factors in the tumor microenvironment.

We have previously demonstrated the use of microfabrication to generate hundreds of uniform breast microtumors with precisely controlled size [53]. As depicted in **Fig. 2A (left panel)**, T47D breast cancer cells, representative of ER+ subtype, were seeded in 150 μm and 600 μm non-adhesive PEGDMA hydrogel microwells. After six days of culture with daily media change, uniform microtumors were obtained as shown in **Fig. 2A (right panel)**.

To establish whether these engineered microtumor models show size-dependent changes in the physicochemical features of the microenvironment as observed in solid tumors *in vivo*, we analysed characteristic features of advanced stage solid tumors such as hypoxia, reactive oxygen species and rate of cellular proliferation. We predicted that large microtumors would show increased levels of hypoxia, ROS and exhibit higher proliferation akin to features of advanced stage breast tumors [36].

Firstly, hypoxia was measured by assessing intratumoral oxygen availability in the microtumor models through addition of Ru-dpp followed by confocal imaging. The fluorescence of Ru-dpp, quenched under normoxic conditions, is enhanced in regions of hypoxia. This principle allows us to visualize spatial distribution of hypoxia in microtumors. Ru-dpp staining (indicated by red) was enhanced to a greater extent in large microtumors in contrast to the smaller ones **(Fig. 2B left panel)**.

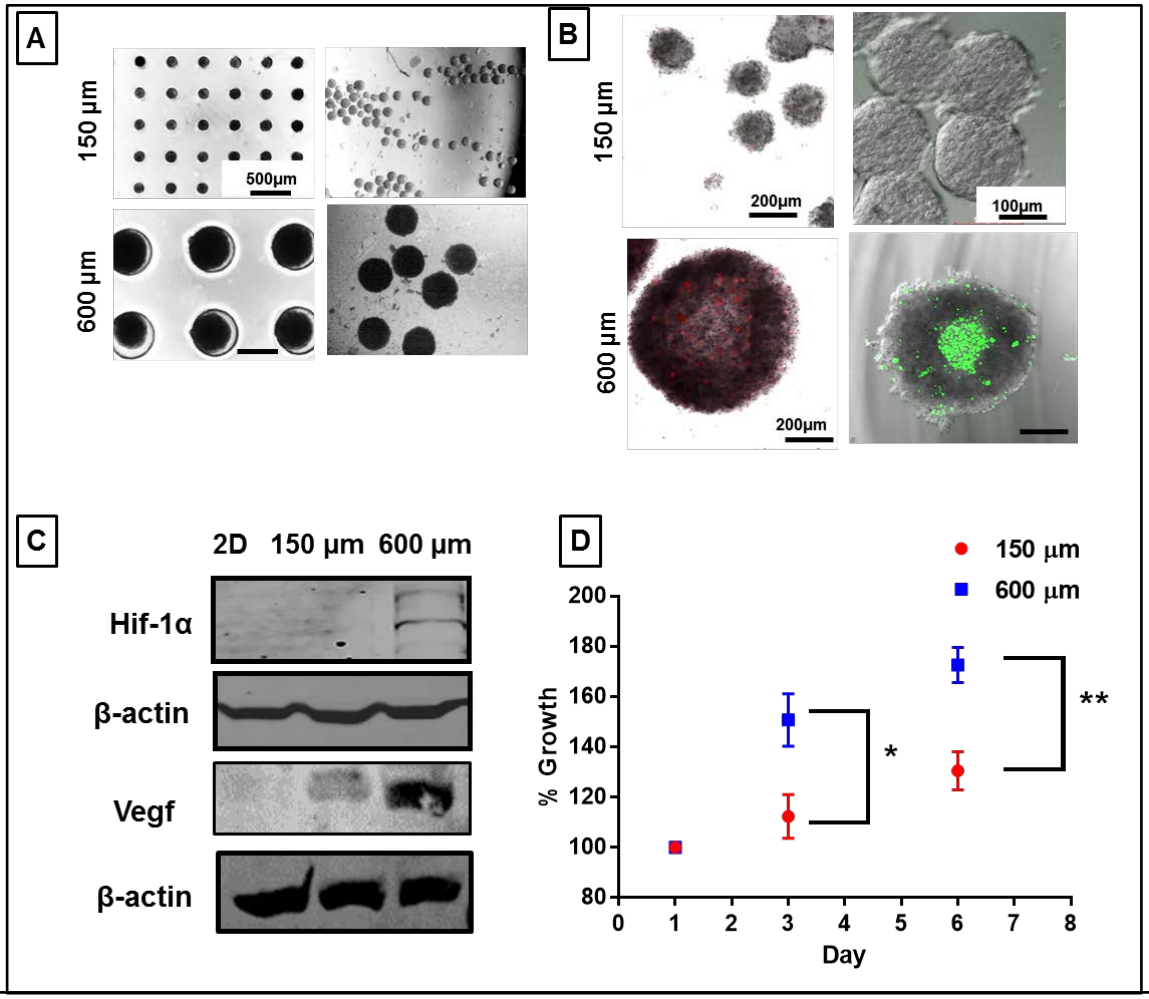

Figure 2: Microtumor size affects physicochemical features of tumor microenvironment

A) T47D cells were cultured in PEGDMA hydrogel array and seeded in devices with, 150 µm and 600 µm size microwells, left panel. Microtumors harvested at day 6 (right panel) represent uniform size microtumors. B) Ru-dpp staining (red color) of microtumors harvested on day 6 revealed heterogeneous presence of hypoxic cells in large (600 µm) microtumors (bottom left) as compared to small (150 µm) small ones (top left). DCHFDA staining of microtumors harvested on day 6 showed negligible ROS signal (green color) in small microtumors (top right) in contrast to the large ones (bottom right). C) Hif-1α and Vegf were found to be upregulated in large microtumors at day 6 by western blotting. D) Large microtumors showed higher percentage growth at day 6 and 3 when normalized to day 1 (measured by metabolic

activity assay) compared to small ones (* $p<0.05$, n=4 devices/group, two-way ANOVA with Tukey's post hoc analysis).

Further, ROS were visualized in the microtumors using the 2', 7' –dichlorofluorescin diacetate (DCHFDA) probe. DCHFDA a non-fluorescent compound, that becomes fluorescent after reaction with hydroxyl and peroxyl ROS. After incubation with DCHFDA for 3 hours, confocal microscopy revealed that large microtumors possessed a central core where ROS (green staining) was detected **(Fig. 2B right panel)**. No ROS production was observed in small microtumors (150 μm).

For further confirming the presence of hypoxia in large microtumors, we measured protein expression of two molecular markers of hypoxia, namely hypoxia inducible factor 1 alpha (Hif-1α) and vascular endothelial growth factor (Vegf). Hif-1α and Vegf have been found clinically to promote tumor progression [57]. Western blotting confirmed the increased expression of Hif-1α in large microtumors (600 μm) as compared to the small ones as well as in 2D cells **(Fig. 2C)**. Vegf, a downstream effector of Hif-1α also had higher expression in large microtumors than small ones (150 μm) **(Fig. 2C)**.

To assess the rate of proliferation in a microtumor model, a standard assay, alamarBlue® assay [54], that measures cellular metabolic activity was used. The enzymatic reduction of resazurin to resorufin by nicotinamide adenine dinucleotide (NADH) dehydrogenase in this assay provides estimate of metabolic activity. Highly metabolically active cells exhibit greater rate of proliferation [54]. The percentage growth (rate of proliferation) of large (600 μm) and small (150 μm) microtumors was calculated by normalizing with their respective metabolic activity on day 1. A two-way ANOVA was performed to test the effects of microtumor size and time (independent variables) on percentage growth of microtumors (dependent variable). There was significant effect of microtumor size on percentage growth of microtumors ($F [1, 18] =22.22$ and $p=0.0002$)

as well as time ($F [2, 18] = 27.81$ and $p<0.0001$). In addition, an interaction between microtumor size and time was found to be significant ($F (2, 18) = 5.591$ and $p=0.0129$). Tukey's post-hoc analysis revealed that large microtumors (600 μm) had significantly higher metabolic activity (**Fig. 2D)** on days 3 and 6, compared to day 1. Importantly, the metabolic activity of large microtumors on days 3 and 6 was significantly higher than that of smaller microtumors.

Taken together, these results indicate that controlling microtumor size can affect the physicochemical features of the tumor microenvironment. Hypoxia, a common feature of advanced solid tumors *in vivo* [58], was found to be upregulated at the molecular level through induction of Hif-1α in large microtumors. Additionally, downstream effector, Vegf, directly linked to this pathway was also elevated in the large microtumors suggesting that large microtumors acquire some of the characteristics of pro-angiogenic tumors, one of the hallmarks of tumor progression [39].

Hypoxic cells have been shown to generate ROS [59] that justifies presence of ROS in large microtumors. However, the interplay between ROS and Hif-1α is complex as studies show that effect of ROS on Hif-1α depends on various factors like degree of hypoxia and forms or intracellular localization of ROS [60]. Metabolic activity assessed by enzymatic reduction assay is a surrogate of cell number and indicator of cellular proliferation [54].

Interestingly, higher rate of proliferation observed in large microtumors as compared to the smaller ones (150 μm) suggest that large microtumors may be considered more aggressive than the small ones. Indeed, clinically advanced stage tumors are reported to possess higher proliferation index [61]. For example, in a large cohort of breast cancer patients, Ki-67, a proliferative marker, was found to be an independent prognostic factor [61]. Patients with Ki-67 less than 15% had significantly greater overall survival than those with Ki-67 with greater than 45%. This indicated that advanced stage patients with lesser survival rates had tumors with higher proliferative index values.

3.2 Three-dimensional cultures of T47D microtumors affect cell cycle progression.

We investigated whether the observed microtumor size-dependent changes in physicochemical factors (hypoxia, ROS) affect their cell cycle progression. We also sought to determine if the size-dependent changes in proliferation as estimated by metabolic activity correlate to their cell cycle progression in these microtumor models. Cell cycle progression from G0/G1 (gap/DNA repair phase), S (synthesis phase) to G2/M (growth/mitotic phase) has been shown to be influenced by the tumor microenvironment [62]. Further, oxidative stress induced in cells can cause DNA damage and arrest of cells in the G0/G1 phase [62]. On the other hand, a higher proliferation index is associated with higher proportion of cells in the G2/M phase [63]. Therefore, it was predicted that large microtumors with a higher rate of metabolic activity would exhibit higher proportion of cells in G2/M phase.

Propidium iodide (PI) staining was performed to determine DNA content in cells and scatter plots were drawn from flow cytometer. In **Fig. 3A**, R1 represents forward *vs.* side scatter that is used to eliminate cell debris. R2 depicts side scatter area *vs.* height, which eliminates doublet populations by considering only cells that fall on the line with slope 1 (angle = 45°). R3 presents PI channel intensity area *vs.* height that helps to distinguish different phases of cell cycle because DNA content increases proportionally to cell cycle phases (2N in G0/G1 phase, 4N in G2/M phase) [62]. Fifteen thousand cells were counted in R3 for all samples. This region is converted to histograms and calculated for % cells in each phase by ModFit software.

The R3 plots showed an increased proportion of cells with much less PI content in large (600 μm) microtumors **(red box, Fig. 3A iii)** compared to 2D cells or small (150 μm) microtumors**.**

A one-way ANOVA was performed to analyze effect of culture conditions (2D, 150 μm and 600

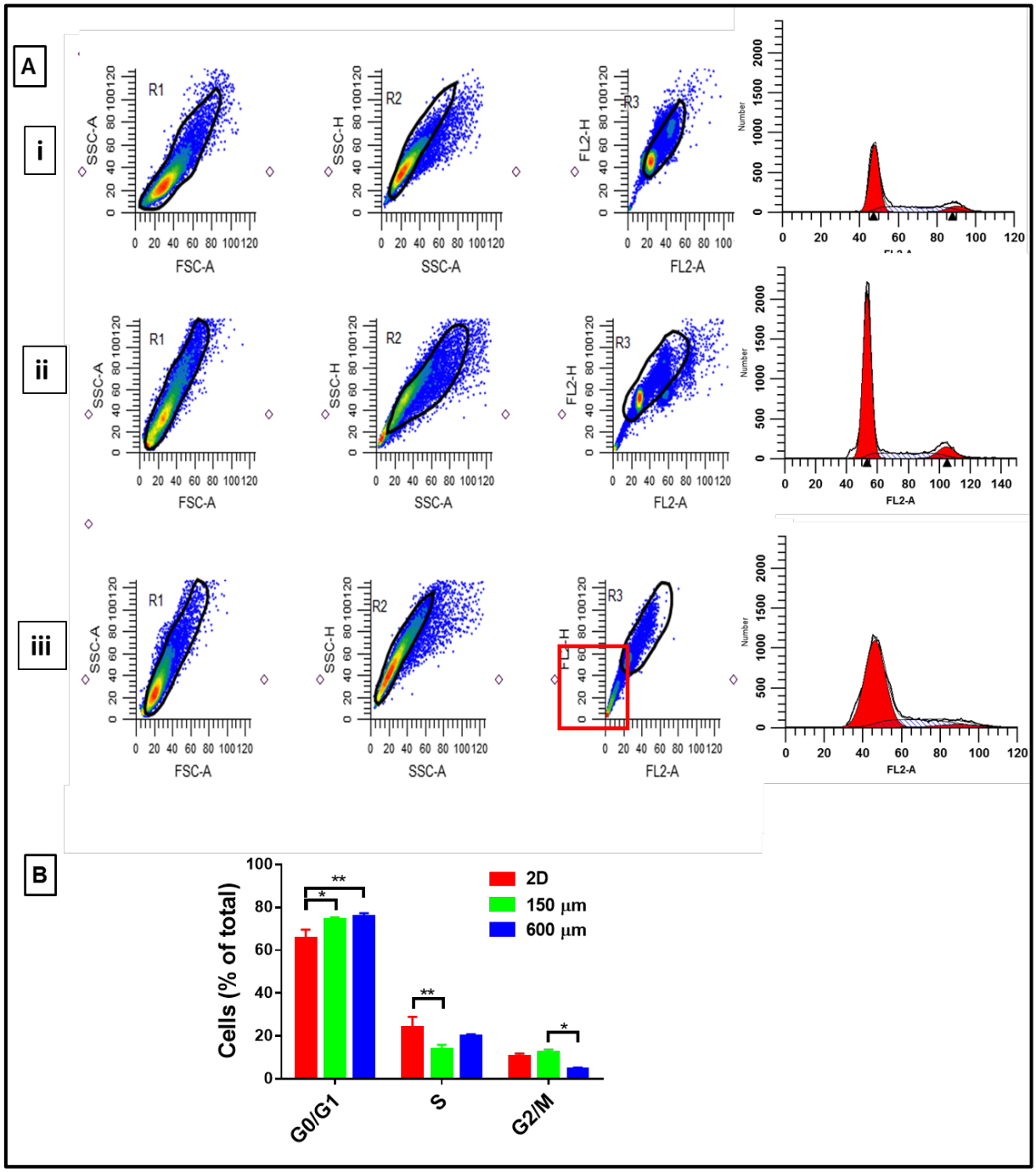

Figure 3: Three dimensional cell culture of T47D affects cell cycle progression

A) Scatter plots of T47D cells cultured for 6 days as 2D (i), small microtumors (ii) and large microtumors (iii). The corresponding histograms are depicted in red. Note that cell number intensity in scatter plots decreases as red>yellow>green>blue. Red box indicates large population with low PI content in R3 for large microtumors (iii). B) Quantification of proportion of cells in each phase showed increased G0/G1 phase in 3D as compared to 2D. Also, decrease in S phase of small microtumors and reduced G2/M phase in large microtumors was observed (*$p<0.05$, n=3, one-way ANOVA, Tukey's post hoc test).

μm microtumor; independent variable) on cell cycle phases (dependent variable). Culture conditions significantly affected proportion of cells in G0/G1 phase ($F [2, 6] =13.53$ and $p=0.006$), S phase ($F [2, 6] =7.873$ and $p=0.021$) and G2/M phase ($F [2, 6] =33.25$ and $p=0.0006$). Results from one-way ANOVA indicated that 3D microtumors consisted of significantly higher (75%) proportion of cells in G0/G1 (gap/DNA repair) phase than those in 2D cells (65%) suggesting more cells in stationary/repair phase when cultured under 3D microtumors **(Fig. 3B).** Tukey's post-hoc test suggested that large microtumors had significantly less number of cells in the G2/M (growth/mitotic) phase compared to smaller ones. The S-phase was reduced to higher extent in small microtumors as compared to 2D.

The higher proportion of cells in G0/G1 phase in 3D cultures compared to 2D can be explained based on the increased barriers for nutrition and oxygen diffusion in 3D model as compared to 2D, causing more DNA damage [62]. It should be noted that contradictory to our predictions, large microtumors also showed decreased percentage of cells in G2/M phase compared to the small ones. The DNA damage may likely be a result of hypoxia and oxidative stress that is experienced by the cells in the core of large microtumors **(depicted in Fig. 2)**. As mentioned previously, oxidative stress-induced damage can make cells quiescent and is a feature of clinically advanced solid tumors [64]. However, extrapolation of this feature to large microtumors

needs to be considered with other factors that affect cell cycle progression, namely, cell number doubling time and synchronization of cell cycles prior to seeding [65].

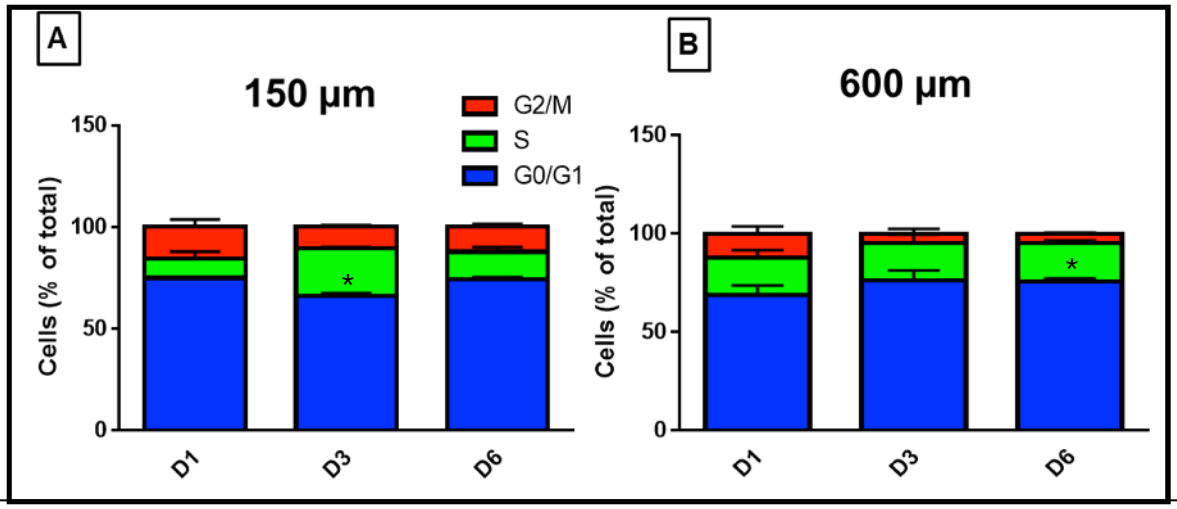

Figure 4: Time dependent changes in the cell cycle progression of microtumors

A) Small microtumors had significantly increased S phase on day 3 compared to other groups. B) Large microtumors had significantly decreased G2/M phase at day 6 compared to other days (*$p<0.05$, n=3, one-way ANOVA, Tukey's post hoc test).

To further evaluate whether observed changes in the cell cycle progression at day 6 could be attributed to time-dependent changes during culture, cell cycle analyses of microtumors harvested at days 1, 3 and 6 were performed. It was predicted that large microtumors would lose G2/M as compared to their day 1 status due to increased oxidative stress with time.

A one-way ANOVA was performed independently for large and small microtumors to analyze effects of time (independent variable) on cell cycle phases (dependent variable). There was significant effect of time and cell cycle phases in small microtumors ($F [2, 6]=125$ and $p<0.0001$) as well as large microtumors ($F [2, 6]=315.8$ and $p<0.0001$). Tukey's post-hoc analysis revealed that large microtumors (600 µm) had significant decrease in G2/M phase on day 6 compared to day 1 providing support that microenvironmental changes such as hypoxia or oxidative stress

may be responsible for reduction in proportion of cells in growth/mitotic phase **(Fig. 4B)**. However, this finding needs to be confirmed by inhibiting oxidative stress in large microtumors and reassessing cell cycle status. In small microtumors (150 µm), there was a significant increase in S-phase at day 3 that reduced at day 6 indicating that they were affected by time-dependent changes during culture.

3.3 Large microtumors acquire aggressive phenotype.

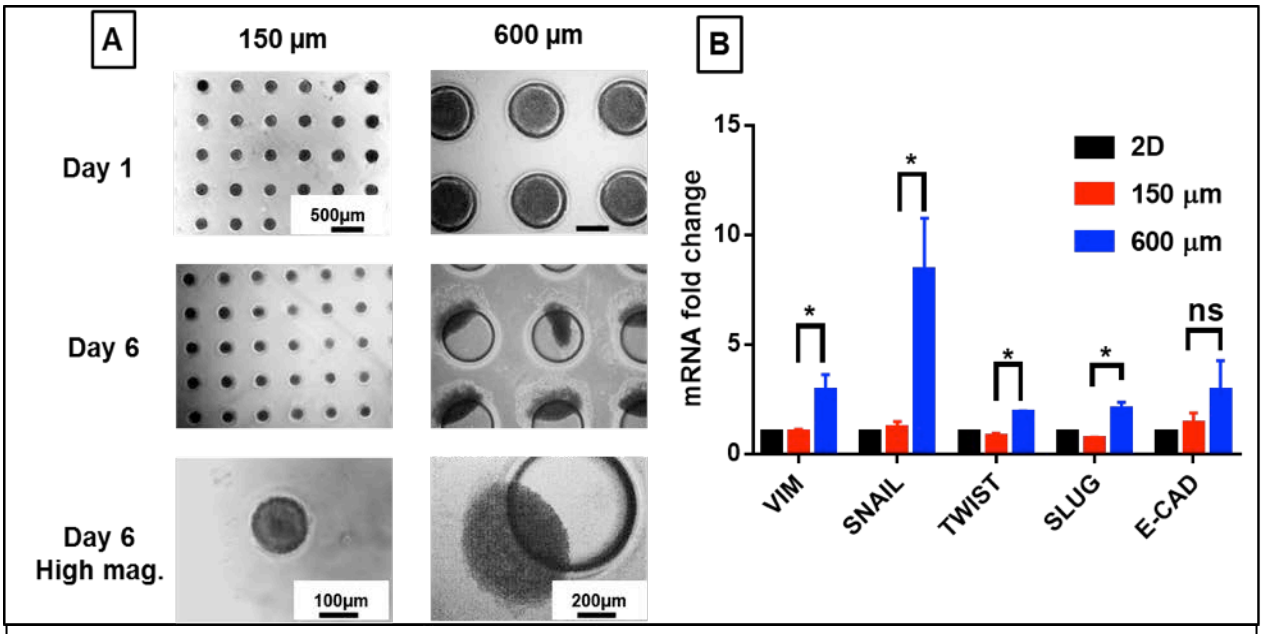

Figure 5: Large microtumors showcase aggressive traits through migratory behaviour and mesenchymal phenotype

A) Large (600 µm) microtumors show migratory behaviour on day 6 unlike small (150 µm) ones. B) Large microtumors had significantly increased VIM, SNAIL, TWIST, SLUG mRNA expression without change in E-Cad as compared to small microtumors (*$p<0.05$, n=3 devices, one-way ANOVA, Tukey's post hoc test).

To test the hypothesis that 600 µm microtumors acquire aggressive phenotype, we evaluated the microscopic changes in large microtumors during 6 days of culture. Interestingly, starting from day 4 up to 6 days of culture, about 85 % of large microtumors migrated out of the PEGDMA hydrogel arrays while the small ones (150 µm) remained intact inside the hydrogel devices **(Fig. 5A)**.

In order to further determine if this observed migration is due to the molecular changes in the signalling pathways reported for classical EMT, gene expression of reported EMT markers including Vimentin, Snail, Slug, Twist and E-Cadherin was measured. Large (600 µm) microtumors were predicted to have an increased level of mesenchymal markers with loss of epithelial marker compared to the smaller (150 µm) ones.

A one-way ANOVA was performed to analyze effect of culture conditions such as 2D, 150 µm and 600 µm microtumors (independent variable) on EMT gene expression (dependent variable). All the tested mesenchymal markers including Vimentin (Vim), Snail, Twist and Slug were significantly affected ($p < 0.05$). However, epithelial marker, E-Cadherin (E-Cad) was not significantly affected ($F [2, 6] = 1.411$ and $p=0.3145$). The Tukey's post-hoc analysis revealed that large microtumors had significant upregulation of mesenchymal markers Vim, Snail, Twist and Slug without loss of epithelial marker, E-Cad as compared to small microtumors.

This observed 'migratory' behaviour or collective cell migration in large microtumors (600 µm) could be linked to the aggressive phenotype of tumors found in advanced stage cancers in the clinic [66]. The upregulation of mesenchymal markers at mRNA level confirmed the mesenchymal transformation of these non-invasive T47D cells when cultured as 600 µm microtumors. Additionally, previous study in these microtumors also demonstrated protein level upregulation of mesenchymal markers, Snail and Vimentin [53]. Interestingly, at both mRNA and protein level, E-Cad levels did not change significantly with microtumor size ($p >0.05$). This depicted that large microtumors did not follow the classical EMT (upregulation of mesenchymal

markers with simultaneous loss of E-Cad). Other studies have also reported that the loss of E-Cad is not a necessity for EMT [67, 68]. This may represent partial EMT phenotype where cells acquire mesenchymal phenotype without loss of epithelial markers like E-Cad. Thus, there could be other mechanisms in large microtumors that are responsible for mesenchymal characteristics while maintaining their epithelial phenotype [69].

This observation is also consistent with the 'collective' or 'cohesive' migration reported in recent studies [38]. This 'migratory' behavior or collective cell migration in large microtumors could be linked to the aggressive phenotype of tumors found in the advanced stage cancers in the clinic [66, 70, 71]. Cumulatively, this suggests that large microtumors of T47D behave similar to the aggressive advanced breast tumors as demonstrated by mesenchymal marker upregulation and migratory phenotype.

3.4 Large T47D microtumors lose ER-α expression at protein level recapitulating observations in clinically advanced tumor samples.

The estrogen receptor alpha (ER-α) is responsible for driving the growth of breast tumors with an ER+ subtype. It has been widely used as a prognostic marker for ER+ breast cancer progression as well as to predict the response to endocrine therapy [72]. Clinically, it is reported that ER-α levels are downregulated or lost at both gene and protein levels with tumor progression [73]. Therefore, we measured transcriptional and translational expression of ER-α in the small and large microtumors.

We observed no significant changes in the ER-α mRNA levels as a function of microtumor size (small 150 μm *vs.* large 600 μm microtumors) and time in culture (days 1, 3 and 6) **(Fig. 6A)**. However, there was a significant loss of ER-α protein expression in the large microtumors at

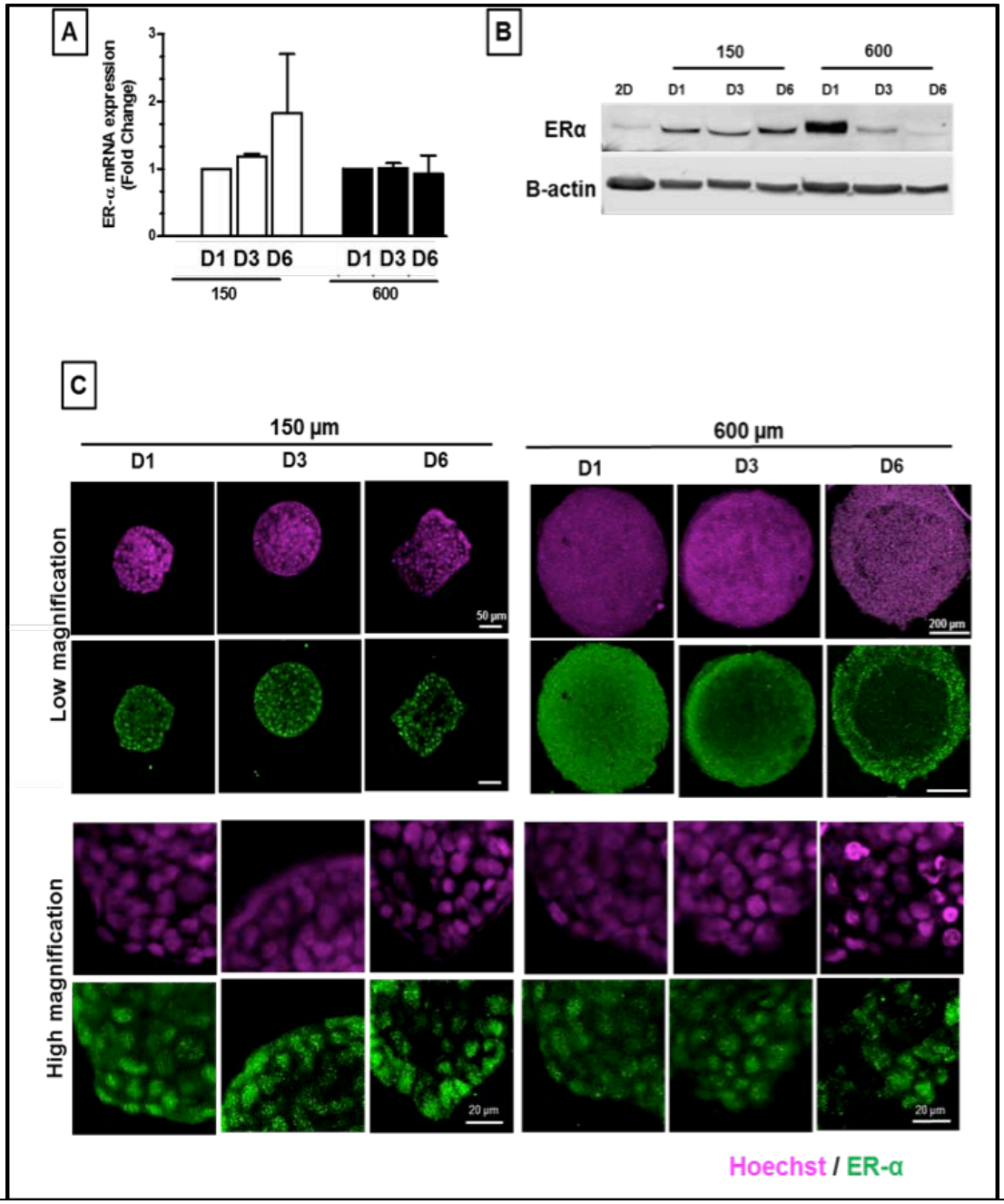

Figure 6: ER-α although unaffected at gene level, is lost at protein level beyond day 3 in large microtumors.

A) ER-α mRNA expression is maintained through all days of culture and not affected by microtumor size. B) ER-α protein expression was lost in the large microtumors beyond day 3. C) ER-α immunofluorescence (green) images (2D projection of maximum intensity) indicated nuclear presence of receptor in the microtumors (high magnification images). Large microtumors revealed loss near the core (second row).

days 3 and 6 **(compared to respective day 1, Fig. 6B).** On the contrary, small microtumors did not show much change in ER-α protein expression from day 1 to day 6.

Previous studies have reported ER-α downregulation with hypoxia in breast cancer cell lines as well as in clinical samples [74, 75]. In these studies, it was demonstrated that Hif-1α induced by hypoxic chambers depleted ER-α protein expression in ER+ cell lines such as MCF-7. Stoner and colleagues investigated the mechanisms for the ER-α receptor downregulation and found proteasome-mediated degradation triggered due to hypoxia as the underlying cause [74]. Thus, loss of ER-α protein in large microtumors may be attributed to the higher levels of hypoxia and Hif-1α present only in the large microtumors **(Fig. 2B and 2C).**

To further establish link between the loss of ER-α in large microtumors and hypoxia, we performed immunofluorescence studies on microtumors cultured for 1, 3 and 6 days. This technique enabled to obtain spatial distribution of ER-α in the microtumors. As shown in **Fig. 6C**, the ER-α expression in small microtumors was maintained through all days of culture except for some loss near the core at day 6, thus confirming our data of protein expression in **Fig. 6B**. On the other hand, large microtumors (600 μm) showed decreased ER-α expression in the core **(Fig. 6C, low magnification panel)** at day 3 and day 6 confirming results of western blotting **(Fig. 6B)**.

As hypoxia was found to be present near the core of large microtumors **(Fig. 2B),** the reduced fluorescence of ER-α signal in the core indicated hypoxia-mediated receptor downregulation as reported in previous studies for hypoxic 2D cultures [74, 75]. It should be noted that this absence of fluorescent signal in the center of large microtumor was not an artefact of staining (such as due to microtumor size-mediated diffusion limitation). Our previous study has shown uniform staining of other proteins such as E-cad throughout the core of the large microtumors [53].

Taken together, these observations offer mechanistic insights into tumor progression of ER+ microtumors as a function of microtumor size. This finding has high clinical significance, as we were able to induce loss of ER-α in large migratory microtumors in real time without affecting ER expression in small ones, both made of same non-invasive T47D cell line. Indeed, clinical studies have reported loss of ER-α, at both gene and protein level as the disease stage progresses from intraductal to invasive carcinomas [73]. About 30% of patients lose ER-α as the disease progresses to later stages [42]. Li and co-workers have demonstrated correlation between ER-α protein and tumor size as well as clinical stage in the patient samples. However, the lack of change in ER-α mRNA over time in both, large and small microtumors suggests that microtumor size does not influence the transcriptional level changes in ER-α.

Cumulatively, these results suggest that ER-α receptor expression in large microtumors is affected by factors such as hypoxia and the loss of expression and establishes their similarity with invasive carcinomas. This similarity with clinical data further validates that the large microtumors (600 μm) show phenotypic traits of advanced stage breast tumors. Importantly, the microtumor models acquire such clinically relevant phenotypic characteristics in the same ER+ cell lines in a real time, without exposure to hypoxic chambers or genetic manipulations.

3.5 Large T47D microtumors exhibit endocrine resistance to 4-OHT treatment.

Our studies so far showed that the large microtumors recapitulate many characteristics of large microtumors with clinically advanced ER+ tumors such as pro-angiogenic behavior, mesenchymal marker upregulation, migratory behavior and more importantly, loss of ER in real time. We explored whether they also exhibited endocrine resistance, another feature of ER+ breast cancer progression [76]. A standard drug of choice in endocrine therapy, 4-

hydroxytamoxifen (4-OHT) was used to treat the microtumors. The concentration of 4-OHT (50 μM) was chosen based on the preliminary data from optimization studies that resulted in an effective inhibition in the growth of microtumors (data not shown). Briefly, both small and large microtumors were cultured in 1x1 cm^2 PEGDMA devices for three days and treated with 50 μM 4-OHT solution from day 3-6. On day 6, this solution was removed and the metabolic activity was analysed via alamarBlue® assay.

A two-tailed t-test revealed that there were significant differences between growth of treated

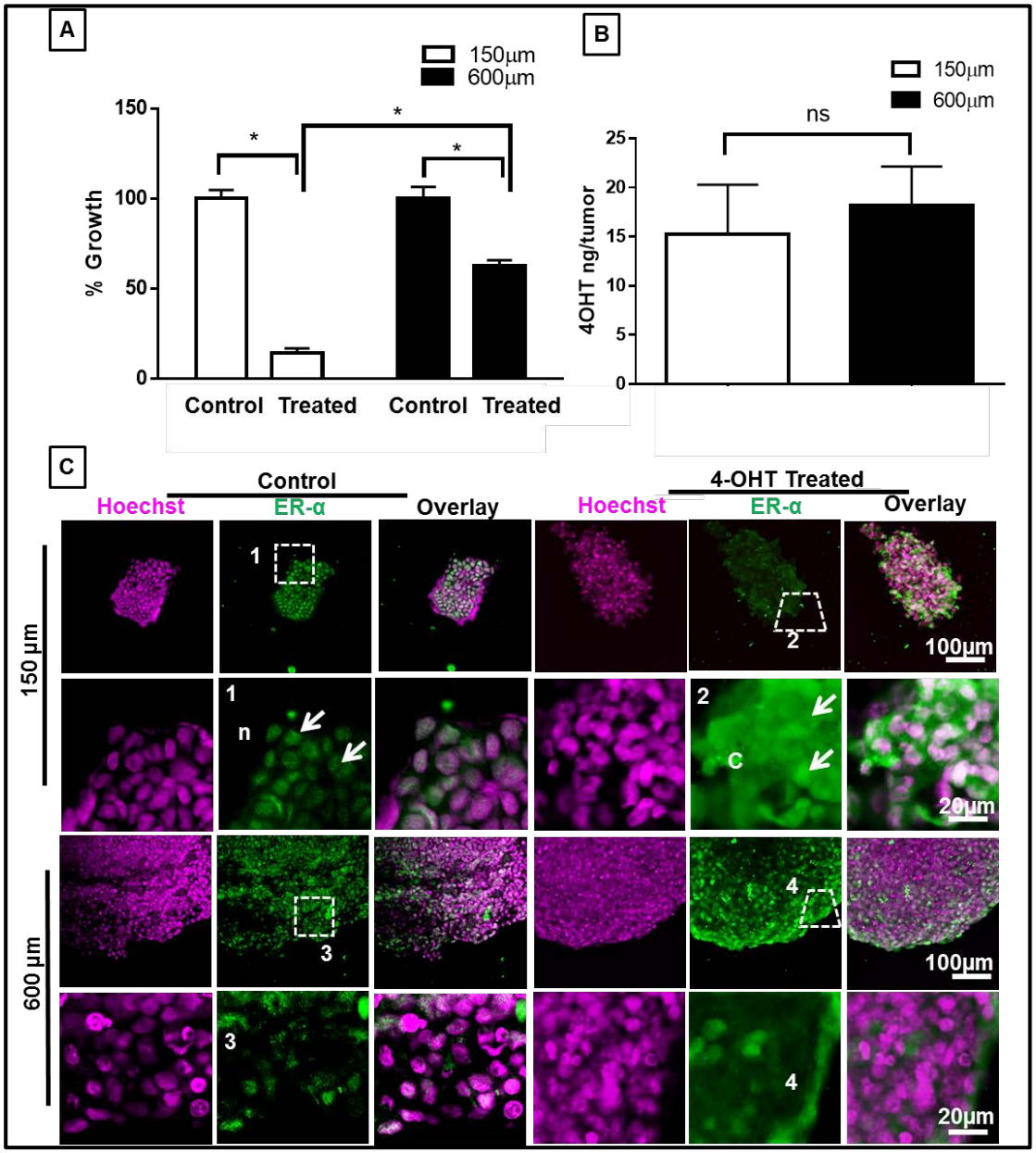

Figure 7: Large (600 μm) microtumors exhibit resistance to 4-OHT treatment.

A) Small (150 μm) microtumors treated with 4-OHT exhibited only 14% of growth compared to their control while the large ones exhibited 65% of growth suggesting that large microtumors develop endocrine resistance (n=7 devices/group, * indicates $p<0.05$, unpaired t-test). B) Quantification of 4-OHT/microtumor through mass spectrometry revealed no significant size-dependent changes in 4-OHT levels in the small *vs.* large microtumors ($p>0.05$, n= 3 devices, unpaired t-test, NS: non-significant). C) ER-α immunofluorescence images of control and treated microtumors showed cytoplasmic presence of ER in the small microtumors after 4-OHT treatment (Row 2, region 2) as compared to controls (Row 2, region 1). While large microtumors did not reveal any such differences (Row 4, regions 4 and 3).

microtumors based on size ($t=31.65$, $df=15$, $p<0.0001$).

The small (150 μm) microtumors treated with 4-OHT exhibited only 14% growth (86% inhibition) compared to that in the vehicle control group **(Fig. 7A)**. In contrast, large microtumors treated with 4-OHT exhibited 65% growth (35% inhibition) of that observed in the vehicle controls. The data indicated that small microtumors were more sensitive to growth inhibition by 4-OHT than the larger ones.

Additionally, we investigated whether the observed differences in the drug response are due to size-dependent diffusion limitations leading to the variable drug levels in small *vs*. large microtumor models. This was addressed by analysing the amount of 4-OHT post-treatment using mass spectrometry. The small and large microtumors treated with 4-OHT were harvested on day 6, followed by addition of Tris-KCl lysis buffer and homogenization. The lysates were run by a mass spectrometer to quantify 4-OHT levels in the microtumors. Results from the t-test summary showed $p=0.4792$, with $t=0.7836$ and degrees of freedom=3.801. This indicated that

there was no significant difference between total amount of 4-OHT/microtumor in small *vs.* large microtumors **(**p=0.4792; **Fig. 7B)**.

Further, to verify if the 4-OHT-induced growth inhibition in small microtumors was due to blockage and stabilization of receptor, immunofluorescence studies were performed on 4-OHT-treated microtumors. Previous studies have demonstrated that ligands such as 4-OHT that can conformationally block ER-α, hinder nuclear translocation and prevent downstream signaling involved in the cell proliferation [77, 78]. The results revealed that ER-α in most cells of 4-OHT-treated small microtumor (150 μm) was not co-localized with nucleus but was localized in the cytoplasmic compartment **(Fig. 7C highlighted area 2)** as compared to untreated controls **(Fig. 7C highlighted area 1)**. However, we observed that overall large microtumors had no clear effect of 4-OHT treatment on ER-α receptor sub-cellular expression.

Due to a significant difference in response to 4-OHT in the small *vs.* large microtumors, we can conclude that 4-OHT treatment is not as effective in inhibiting growth of large microtumors as in the small ones. One of the crucial mechanisms for observed endocrine resistance in large microtumors (600 μm) could be the loss of ER-α, which is the target of 4-OHT **(Fig. 6B).** It is obvious that as the drug target decreases from day 3 in large microtumors, the sensitivity to drug is bound to diminish. As highlighted by Osborne and Schiff [76], one of the most common explanations for endocrine resistance with ER+ breast cancer progression in clinic is loss of ER-α. Therefore, these observations together indicate that the endocrine resistance in large microtumors may be due to the loss of the target ER-α from day 3 to day 6.

It should be noted that the drug amount of 4-OHT per microtumor was not significantly different in small *vs.* large microtumors and may not have influenced the drug influence the response (**Fig. 7A**). However, it is important to consider that in an equal volume of cell lysates, the number of small microtumors (150 μm) is nearly 4- fold more than the large ones (600 μm) (data not shown). Thus, drug content normalized with respect to the number of microtumors showed

similar 4-OHT levels (**Fig. 7B**). When 4-OHT content was normalized to the total number of cells to determine amount of 4-OHT per cell, it was seen that large microtumors had significantly lower amount of drug compared to the smaller ones (data not shown). This indicated that although amount of 4-OHT/microtumor is not significantly different, either all cells in large microtumors had taken up less amount of drug or there was heterogeneity in the drug uptake throughout the large microtumor. Given that different regions within the microtumor experience varied physiological milieu, it might be worthwhile to investigate if certain region (periphery or core) preferentially take up the drug. Reduced drug uptake in large microtumors (600 µm) may be also be a cumulative effect of efflux pumps such as P-glycoprotein or multidrug resistance-associated protein, upregulated in large microtumors that may result in lower amount of drug/cell and needs further investigation [79].

3.6 Large T47D microtumors display unique trend in the growth factor receptor signalling.

As large microtumors lose dependence on ER-α for survival and progression, we explored other proliferation pathways that could have contributed to their growth and aggressive phenotype. From literature, it is quite common to find dependence of clinically advanced stage tumors on the growth factor or receptor tyrosine kinase pathways such as Human Epidermal Growth Factor Receptor (EGFR/HER2) and Insulin Growth Factor Receptor (IGFR) [80]. Crosstalk with ER-α or independent activation of growth factor receptors could also lead to activation of downstream pathways that are frequently involved in breast tumor progression and metastasis clinically [81].

We investigated whether large microtumors were dependent on EGFR/HER2, widely reported pathway activated in ER+ advanced breast cancer [82]. We hypothesized that while small microtumors are dependent on ER-α for survival, large ones (600 μm) acquire growth factor receptor activation, which could further contribute to their migratory phenotype **(Fig. 8A)**. Protein

analysis of upstream and downstream receptors of EGFR pathway was investigated in both, small and large microtumors. Western blotting indicated similar levels of phosphorylated EGFR (activated receptor form) at tyrosine residue, 845 in the small and large microtumors over 6 days of culture **(Fig. 8B)**. Interestingly, it was found that total EGFR levels decreased

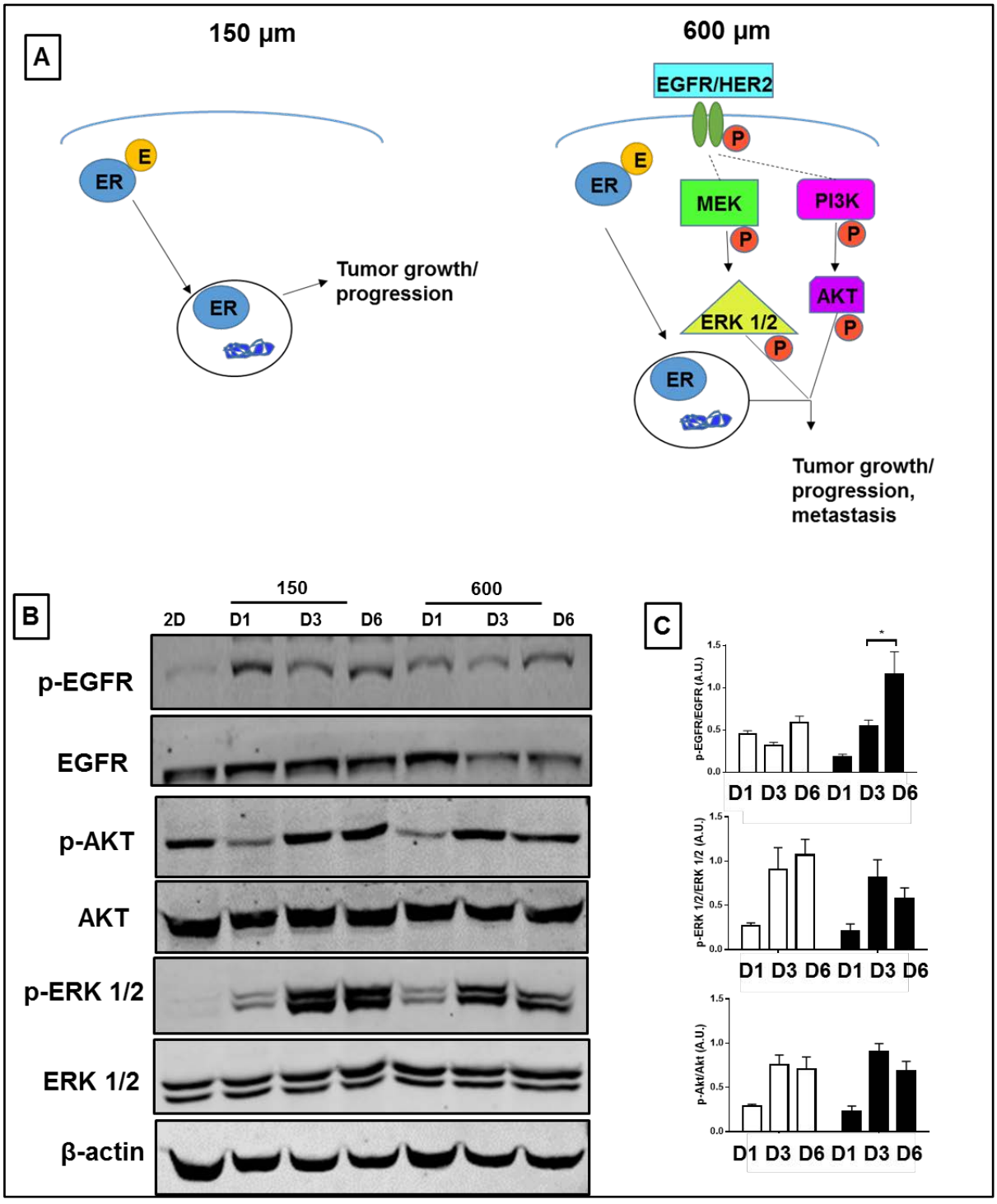

Figure 8: Large microtumors display unique growth factor receptor signalling

A) Schematic showing alternative proliferative pathways in the microtumor model. B) Western blotting for key molecules in growth factor receptor signalling shows higher levels of p-EGFR/Total EGFR in large microtumors. C) Densitometry analysis depicts significant upregulation of p-EGFR/total EGFR in large ones, whereas p-Akt/Akt or p-ERK/ERK was upregulated in both small and large microtumors in a time-dependent manner. They did not show significant effect of microtumor size. (n=3-5 experiments, * indicates $p<0.05$, two-way ANOVA). Note, white bars indicate small microtumors while black bars depict large ones.

significantly on day 3 and 6 in large microtumors, but not in the smaller ones.

A two-way ANOVA was performed to test the effect of microtumor size and time (independent variables) on protein expression of microtumors. There was significant effect of time on pEGFR/EGFR expression ($F [2, 12] =11.96$ and $p=0.0014$) but not of microtumor size ($F [1, 12] =3.137$ and $p=0.1019$). However, there was significant interaction between microtumor size and time ($F [2, 12] =6.184$ and $p=0.0143$). For pAkt/Akt, there was significant effect of time ($F [2, 12] =18.99$ and $p=0.0002$) but not of microtumor size ($F [1, 12] =0.09$ and $p=0.761$). Also, there was no significant interaction between microtumor size and time ($F [2, 12] =0.6228$ and $p=0.5529$). For pERK/ERK, there was significant effect of time ($F [2, 12] =14.56$ and $p=0.0006$) but not of microtumor size ($F [1, 12] =2.328$ and $p=0.153$). In addition, there was no significant interaction between microtumor size and time ($F [2, 12] =0.521$ and $p=0.6067$).

Overall, activation of EGFR pathway depicted by the ratio of p-EGFR/total EGFR levels suggests significant increase from day 3 to day 6 in large microtumors **(Fig. 8C)**. This implies that even though p-EGFR levels were not microtumor size-dependent, the activation of EGFR pathway was affected by loss of total EGFR expression in large microtumors (600 µm) from day 3 to day 6.

In order to study if downstream effectors of EGFR pathway are also affected in microtumor size-dependent manner, protein expression and phosphorylation of protein kinase B (Akt) and extracellular regulated kinase (ERK 1/2) were studied in these microtumors. As shown in **Fig. 8B,** Akt was activated through increased levels of p-Akt/total Akt at serine 473 on days 3 and 6 in both, small and large microtumors. Similarly, small and large microtumors had ERK 1/2 activation (pERK 1/2/total ERK 1/2) at day 3 and 6 higher than day 1 ($F [2, 12] =14.56$, $p=0.0006$) due to increased levels of p-ERK 1/2 (Threonine 404/ Tyrosine 402). However, small microtumors (150 μm) had similar p-Akt/Akt and p-ERK 1/2/ ERK1/2 levels at day 3 and day 6 as the large ones (**Fig. 8C**).

The trend in EGFR expression of large (600 μm) microtumors is unlike many studies that report over-expression of EGFR in hypoxic tumors [83]. This observation needs to be investigated further. The downstream receptor analysis suggested that activation of these receptor kinase pathways are not dependent on microtumor size even though they show time-dependent changes. However, loss of EGFR suggests that the large microtumors could be using this pathway for adaptive mechanisms leading to aggressive behaviour and endocrine resistance [84].

4. CONCLUSIONS AND FUTURE DIRECTIONS

We have developed *in vitro* size-controlled microtumor models that recapitulate important hallmarks of breast tumor progression such as hypoxic microenvironment, pro-angiogenic factor (Vegf) secretion, loss of ER-α, upregulation of mesenchymal makers without loss of epithelial cadherin (E-cad) and migratory phenotype just by controlling microtumor size in the same cell line. This model was well characterized for its ability to recapitulate early and advanced stage of the disease through upregulation of ROS, hypoxia and molecular markers (Hif-1α and Vegf) in the large microtumors in contrast to the small ones. In addition, hypoxia and oxidative stress-induced damage was resulted in decrease in actively dividing population of cells in large microtumors (600 μm). Clinically observed feature such as collective cell migration further validated the utility of model for studying cancer biology and therapeutics.

Further, the ER-α regulating proliferation in ER+ cells was downregulated in the large microtumors. Though no changes were observed in mRNA levels, large microtumors had decreased protein levels of ER-α over time unlike small ones. This loss in expression was linked to the hypoxia-mediated proteosomal degradation of ER. Additionally, large microtumors exhibited endocrine resistance to ER-targeted 4-OHT in contrast to small ones. Taken together, acquired mesenchymal phenotype, migratory phenotype, loss of ER-α, and endocrine resistance observed in large microtumors (600 μm) established the clinical relevance of these novel *in vitro* models due to their ability to recapitulate some of the clinical signatures of disease progression. On the other hand, small (150 μm) microtumors fabricated from the same non-invasive cell line and minimal phenotypic changes serve as a 3D control of early stage, non-

aggressive disease, making these models more powerful for interrogating biological mechanisms involved in tumor progression.

Despite these studies, many mechanisms may exist that play an essential role in generating global phenomenon such as drug resistance and collective cell migration observed in the large microtumors. In order to study alternative growth pathways in large/aggressive tumors, status of growth factor receptor pathways was investigated. However, we observed that though upstream receptor (EGFR) was preferentially activated in large microtumors, downstream pathways such as Akt and ERK1/2 did not show any difference in the activation levels between small and large microtumors. Thus, future studies are required to delineate the mechanisms by which total EGFR protein levels are downregulated in large microtumors and alternative mechanisms that large microtumors utilize for showing aggressive traits and disease progression. Identification of these targets will enable efficient use of known inhibitors of these pathways and their combinations thereof to treat the aggressive tumors and demonstrate therapeutic benefit.

In conclusion, recapitulation of growth-dependent changes in the physicochemical features of *in vivo* solid tumor microenvironment and acquisition of mesenchymal phenotype in the large microtumors were achieved using a single non-invasive T47D cell line. When cultured in non-adhesive PEG hydrogel microwells, precise control over microtumor size enabled controlled changes in the microtumor microenvironment in a reproducible manner in both small and large microtumors. Such precise control over microenvironment further triggered underlying signaling mechanisms to capture phenotypic differentiation characteristic of early and late-stage disease in small (150 μm) and large (600 μm) microtumors, respectively just by changing the microtumor size alone and without any other artificial culture conditions. The use of the same cell line throughout these studies to mimic different stages of disease is of further importance.

Taken together, one of the novel and significant findings of the studies presented in this thesis is that by manipulating tumor size (and size alone), we were able to produce 3D cultures that reflect different stages of tumor progression as revealed by different measures, all derived from

the same cells. This demonstrates that size alone is sufficient to bring about this transformation of non-invasive cells to aggressive migratory phenotypes in 3D cultures. This is of further significance in various cancer studies mainly because it eliminates the need to use different cell lines to study tumors at different stages of disease.

Therefore, these *in vitro* models are better than currently used approaches of gene manipulations, artificial culture conditions or use of different cell lines to represent the disease stage. These *in vitro* models can be used to screen drugs or develop better therapies in a stage-specific manner unlike currently used cell culture models. However, these microtumor models also possess some limitations. Fabrication of polymeric moulds that generate arrays on hydrogels is a complicated procedure that requires expertise. In addition, many conventional cell-based assays optimized for 2D culture require further optimization for 3D culture to remove effects such as penetration limitation for the assay reagents. These models also lack extracellular matrix and stromal cells that are integral part of the in vivo tumor microenvironment. Nonetheless, the model is an advance over other models in several important ways such as uniformity and precise control over microtumor size, reproducibility, ability to capture tumor progression over a short duration of 6 days. All these advantages will easily allow incorporation of other microenvironmental factors to create more complex and realistic tumor microenvironments that exist *in vivo.*

APPENDIX A

ABBREVIATIONS

Term	Abbreviation
ECM	Extracellular Matrix
ER-α	Estrogen Receptor alpha
4-OHT	4-Hydroxytamoxifen
EMT	Epithelial to Mesenchymal Transition
VIM	Vimentin
E-CAD	E-Cadherin
Hif-1α	Hypoxia inducible factor 1 alpha
ROS	Reactive oxygen species

BIBLIOGRAPHY

1. Hanahan, D. and Robert A. Weinberg, *Hallmarks of Cancer: The Next Generation.* Cell, 2011. **144**(5): p. 646-674.
2. Haycock, J., *3D Cell Culture: A Review of Current Approaches and Techniques*, in *3D Cell Culture*, J.W. Haycock, Editor 2011, Humana Press. p. 1-15.
3. Abbott, A., *Cell culture: Biology's new dimension.* Nature, 2003. **424**(6951): p. 870-872.
4. Yamada, K.M. and E. Cukierman, *Modeling Tissue Morphogenesis and Cancer in 3D.* Cell, 2007. **130**(4): p. 601-610.
5. Mehta, G., et al., *Opportunities and Challenges for use of Tumor Spheroids as Models to Test Drug Delivery and Efficacy.* Journal of controlled release : official journal of the Controlled Release Society, 2012. **164**(2): p. 192-204.
6. Helmlinger, G., et al., *Interstitial pH and pO2 gradients in solid tumors in vivo: high-resolution measurements reveal a lack of correlation.* Nat Med, 1997. **3**(2): p. 177-82.
7. Justice, B.A., N.A. Badr, and R.A. Felder, *3D cell culture opens new dimensions in cell-based assays.* Drug Discovery Today, 2009. **14**(1–2): p. 102-107.
8. Lei, X.-h., et al., *NASA-Approved Rotary Bioreactor Enhances Proliferation of Human Epidermal Stem Cells and Supports Formation of 3D Epidermis-Like Structure.* PLoS ONE, 2011. **6**(11): p. e26603.
9. Moeller, H.-C., et al., *A microwell array system for stem cell culture.* Biomaterials, 2008. **29**(6): p. 752-763.
10. Fennema, E., et al., *Spheroid culture as a tool for creating 3D complex tissues.* Trends Biotechnol, 2013. **31**(2): p. 108-15.
11. Okawa, T., et al., *The functional interplay between EGFR overexpression, hTERT activation, and p53 mutation in esophageal epithelial cells with activation of stromal fibroblasts induces tumor development, invasion, and differentiation.* Genes Dev, 2007. **21**(21): p. 2788-803.
12. Karp, J.M., P.D. Dalton, and M.S. Shoichet, *Scaffolds for Tissue Engineering.* MRS Bulletin, 2003. **28**(04): p. 301-306.
13. Wang, C., et al., *Three-dimensional in vitro cancer models: a short review.* Biofabrication, 2014. **6**(2): p. 022001.
14. Kim, J.B., *Three-dimensional tissue culture models in cancer biology.* Semin Cancer Biol, 2005. **15**(5): p. 365-77.
15. Gurski, L.A., et al., *Hyaluronic Acid-Based Hydrogels as 3D Matrices for in Vitro Evaluation of Chemotherapeutic Drugs Using Poorly Adherent Prostate Cancer Cells.* Biomaterials, 2009. **30**(30): p. 6076-6085.
16. Chignola, R., et al., *Forecasting the growth of multicell tumour spheroids: implications for the dynamic growth of solid tumours.* Cell Proliferation, 2000. **33**(4): p. 219-229.
17. Longati, P., et al., *3D pancreatic carcinoma spheroids induce a matrix-rich, chemoresistant phenotype offering a better model for drug testing.* BMC Cancer, 2013. **13**(1): p. 95.
18. Dhiman, H.K., A.R. Ray, and A.K. Panda, *Three-dimensional chitosan scaffold-based MCF-7 cell culture for the determination of the cytotoxicity of tamoxifen.* Biomaterials, 2005. **26**(9): p. 979-986.
19. Cheema, U., et al., *Spatially defined oxygen gradients and vascular endothelial growth factor expression in an engineered 3D cell model.* Cellular and Molecular Life Sciences, 2008. **65**(1): p. 177-186.

20. Yamazaki, D., S. Kurisu, and T. Takenawa, *Involvement of Rac and Rho signaling in cancer cell motility in 3D substrates.* Oncogene, 2009. **28**(13): p. 1570-1583.
21. Fischbach, C., et al., *Engineering tumors with 3D scaffolds.* Nat Methods, 2007. **4**(10): p. 855-60.
22. Kimlin, L.C., G. Casagrande, and V.M. Virador, *In vitro three-dimensional (3D) models in cancer research: An update.* Molecular Carcinogenesis, 2013. **52**(3): p. 167-182.
23. Kievit, F.M., et al., *Chitosan–alginate 3D scaffolds as a mimic of the glioma tumor microenvironment.* Biomaterials, 2010. **31**(22): p. 5903-5910.
24. Fong, E.L.S., et al., *Modeling Ewing sarcoma tumors in vitro with 3D scaffolds.* Proceedings of the National Academy of Sciences, 2013. **110**(16): p. 6500-6505.
25. Ravi, M., et al., *3D Cell Culture Systems: Advantages and Applications.* Journal of Cellular Physiology, 2015. **230**(1): p. 16-26.
26. Alberts, D., et al., *Originally published as Volume 2, Issue 8190IN-VITRO CLONOGENIC ASSAY FOR PREDICTING RESPONSE OF OVARIAN CANCER TO CHEMOTHERAPY.* The Lancet, 1980. **316**(8190): p. 340-342.
27. Rotem, A., et al., *Alternative to the soft-agar assay that permits high-throughput drug and genetic screens for cellular transformation.* Proceedings of the National Academy of Sciences of the United States of America, 2015. **112**(18): p. 5708-5713.
28. Tung, Y.C., et al., *High-throughput 3D spheroid culture and drug testing using a 384 hanging drop array.* Analyst, 2011. **136**(3): p. 473-8.
29. IWASE, Y., et al., *A Biomimicking Tumor Tissue Model Using Hepatocellular Carcinoma Cell Sheet in a Collagen Sandwich System.* Anticancer Research, 2015. **35**(12): p. 6481-6486.
30. Shin, C.S., et al., *Development of an in vitro 3D tumor model to study therapeutic efficiency of an anticancer drug.* Mol Pharm, 2013. **10**(6): p. 2167-75.
31. Weigelt, B., et al., *HER2 signaling pathway activation and response of breast cancer cells to HER2-targeting agents is dependent strongly on the 3D microenvironment.* Breast Cancer Res Treat, 2010. **122**(1): p. 35-43.
32. Zhang, Y., et al., *Histamine-functionalized copolymer micelles as a drug delivery system in 2D and 3D models of breast cancer.* Journal of Materials Chemistry B, 2015. **3**(12): p. 2472-2486.
33. Colley, H.E., et al., *Polymersome-mediated delivery of combination anticancer therapy to head and neck cancer cells: 2D and 3D in vitro evaluation.* Mol Pharm, 2014. **11**(4): p. 1176-88.
34. Bissell, M.J., *The differentiated state of normal and malignant cells or how to define a "normal" cell in culture.* Int Rev Cytol, 1981. **70**: p. 27-100.
35. Weigelt, B., J.L. Peterse, and L.J. van't Veer, *Breast cancer metastasis: markers and models.* Nat Rev Cancer, 2005. **5**(8): p. 591-602.
36. Place, A.E., S. Jin Huh, and K. Polyak, *The microenvironment in breast cancer progression: biology and implications for treatment.* Breast Cancer Research, 2011. **13**(6): p. 1-11.
37. Nakajima, S., et al., *N-cadherin expression and epithelial-mesenchymal transition in pancreatic carcinoma.* Clin Cancer Res, 2004. **10**(12 Pt 1): p. 4125-33.
38. Friedl, P. and D. Gilmour, *Collective cell migration in morphogenesis, regeneration and cancer.* Nat Rev Mol Cell Biol, 2009. **10**(7): p. 445-457.
39. Kerbel, R.S., *Tumor angiogenesis: past, present and the near future.* Carcinogenesis, 2000. **21**(3): p. 505-515.
40. Ali, S. and R.C. Coombes, *Estrogen Receptor Alpha in Human Breast Cancer: Occurrence and Significance.* Journal of Mammary Gland Biology and Neoplasia, 2000. **5**(3): p. 271-281.
41. Cowell, C.F., et al., *Progression from ductal carcinoma in situ to invasive breast cancer: revisited.* Mol Oncol, 2013. **7**(5): p. 859-69.
42. Osborne, C.K. and R. Schiff, *MECHANISMS OF ENDOCRINE RESISTANCE IN BREAST CANCER.* Annual review of medicine, 2011. **62**: p. 233-247.

43. Roop, R.P. and C.X. Ma, *Endocrine resistance in breast cancer: molecular pathways and rational development of targeted therapies.* Future Oncology, 2012. **8**(3): p. 273-292.
44. Montemurro, F., S. Di Cosimo, and G. Arpino, *Human epidermal growth factor receptor 2 (HER2)-positive and hormone receptor-positive breast cancer: new insights into molecular interactions and clinical implications.* Annals of Oncology, 2013.
45. Taube, J.H., et al., *Core epithelial-to-mesenchymal transition interactome gene-expression signature is associated with claudin-low and metaplastic breast cancer subtypes.* Proc Natl Acad Sci U S A, 2010. **107**(35): p. 15449-54.
46. George, A.L., et al., *Hypoxia and estrogen are functionally equivalent in breast cancer-endothelial cell interdependence.* Molecular Cancer, 2012. **11**(1): p. 1-12.
47. Carlsten, M. and R.W. Childs, *Genetic Manipulation of NK Cells for Cancer Immunotherapy: Techniques and Clinical Implications.* Frontiers in Immunology, 2015. **6**: p. 266.
48. Mak, I.W.Y., N. Evaniew, and M. Ghert, *Lost in translation: animal models and clinical trials in cancer treatment.* American Journal of Translational Research, 2014. **6**(2): p. 114-118.
49. Denayer, T., T. Stöhr, and M. Van Roy, *Animal models in translational medicine: Validation and prediction.* New Horizons in Translational Medicine, 2014. **2**(1): p. 5-11.
50. Jawhar, N.M.T., *Tissue Microarray: A rapidly evolving diagnostic and research tool.* Annals of Saudi Medicine, 2009. **29**(2): p. 123-127.
51. Narod, S.A., *Tumour size predicts long-term survival among women with lymph node-positive breast cancer.* Current Oncology, 2012. **19**(5): p. 249-253.
52. Singh, M., et al., *Production of Uniform 3D Microtumors in Hydrogel Microwell Arrays for Measurement of Viability, Morphology, and Signaling Pathway Activation.* Assay Drug Dev Technol, 2015. **13**(9): p. 570-83.
53. Singh, M., et al., *Three-Dimensional Breast Cancer Models Mimic Hallmarks of Size-Induced Tumor Progression.* Cancer Research, 2016. **76**(13): p. 3732-3743.
54. Al-Nasiry, S., et al., *The use of Alamar Blue assay for quantitative analysis of viability, migration and invasion of choriocarcinoma cells.* Human Reproduction, 2007. **22**(5): p. 1304-1309.
55. Patel, A., et al., *Carbon-based hierarchical scaffolds for myoblast differentiation: Synergy between nano-functionalization and alignment.* Acta Biomaterialia, 2016. **32**: p. 77-88.
56. Livak, K.J. and T.D. Schmittgen, *Analysis of relative gene expression data using real-time quantitative PCR and the 2(-Delta Delta C(T)) Method.* Methods, 2001. **25**(4): p. 402-8.
57. Greijer, A.E. and E. van der Wall, *The role of hypoxia inducible factor 1 (HIF-1) in hypoxia induced apoptosis.* Journal of Clinical Pathology, 2004. **57**(10): p. 1009-1014.
58. Bos, R., et al., *Levels of hypoxia-inducible factor-1α during breast carcinogenesis.* J Natl Cancer Inst, 2001. **93**.
59. LeBrasseur, N., *Hypoxic reaction to reactive oxygen.* The Journal of Cell Biology, 2007. **177**(6): p. 945a.
60. Qutub, A.A. and A.S. Popel, *Reactive Oxygen Species Regulate Hypoxia-Inducible Factor 1α Differentially in Cancer and Ischemia.* Molecular and Cellular Biology, 2008. **28**(16): p. 5106-5119.
61. Inwald, E.C., et al., *Ki-67 is a prognostic parameter in breast cancer patients: results of a large population-based cohort of a cancer registry.* Breast Cancer Research and Treatment, 2013. **139**(2): p. 539-552.
62. Fleisig, H. and J. Wong, *Measuring Cell Cycle Progression Kinetics with Metabolic Labeling and Flow Cytometry.* Journal of Visualized Experiments : JoVE, 2012(63): p. 4045.
63. van Diest, P.J., E. van der Wall, and J.P.A. Baak, *Prognostic value of proliferation in invasive breast cancer: a review.* Journal of Clinical Pathology, 2004. **57**(7): p. 675-681.

64. Reynolds, T.Y., S. Rockwell, and P.M. Glazer, *Genetic Instability Induced by the Tumor Microenvironment.* Cancer Research, 1996. **56**(24): p. 5754-5757.
65. Schorl, C. and J.M. Sedivy, *Analysis of Cell Cycle Phases and Progression in Cultured Mammalian Cells.* Methods (San Diego, Calif.), 2007. **41**(2): p. 143-150.
66. van Zijl, F., G. Krupitza, and W. Mikulits, *Initial steps of metastasis: Cell invasion and endothelial transmigration.* Mutation Research/Reviews in Mutation Research, 2011. **728**(1–2): p. 23-34.
67. Liu, X., et al., *Loss of E-cadherin and epithelial to mesenchymal transition is not required for cell motility in tissues or for metastasis.* Tissue Barriers, 2014. **2**(4): p. e969112.
68. Hollestelle, A., et al., *Loss of E-cadherin is not a necessity for epithelial to mesenchymal transition in human breast cancer.* Breast Cancer Res Treat, 2013. **138**(1): p. 47-57.
69. Son, H. and A. Moon, *Epithelial-mesenchymal Transition and Cell Invasion.* Toxicological Research, 2010. **26**(4): p. 245-252.
70. Wolf, K., et al., *Multi-step pericellular proteolysis controls the transition from individual to collective cancer cell invasion.* Nat Cell Biol, 2007. **9**(8): p. 893-904.
71. Kabla, A.J., *Collective cell migration: leadership, invasion and segregation.* Journal of The Royal Society Interface, 2012. **9**(77): p. 3268-3278.
72. Weigel, M.T. and M. Dowsett, *Current and emerging biomarkers in breast cancer: prognosis and prediction.* Endocrine-Related Cancer, 2010. **17**(4): p. R245-R262.
73. Kurebayashi, J., et al., *Expression Levels of Estrogen Receptor-α, Estrogen Receptor-β, Coactivators, and Corepressors in Breast Cancer.* American Association for Cancer Research, 2000. **6**(2): p. 512-518.
74. Stoner, M., et al., *Hypoxia induces proteasome-dependent degradation of estrogen receptor alpha in ZR-75 breast cancer cells.* Mol Endocrinol, 2002. **16**(10): p. 2231-42.
75. Liu, G.Y., et al., *[Hypoxia induces down-regulation of estrogen receptor alpha in human breast cancer].* Zhonghua Zhong Liu Za Zhi, 2004. **26**(11): p. 664-8.
76. Osborne, C.K. and R. Schiff, *Mechanisms of endocrine resistance in breast cancer.* Annu Rev Med, 2011. **62**: p. 233-47.
77. Kocanova, S., et al., *Ligands specify estrogen receptor alpha nuclear localization and degradation.* BMC Cell Biology, 2010. **11**(1): p. 1-13.
78. Long, X., M. Fan, and K.P. Nephew, *Estrogen receptor-alpha-interacting cytokeratins potentiate the antiestrogenic activity of fulvestrant.* Cancer Biology & Therapy, 2010. **9**(5): p. 389-396.
79. Ring, A. and M. Dowsett, *Mechanisms of tamoxifen resistance.* Endocrine-Related Cancer, 2004. **11**(4): p. 643-658.
80. Nicholson, R.I., et al., *Modulation of epidermal growth factor receptor in endocrine-resistant, oestrogen receptor-positive breast cancer.* Endocrine-Related Cancer, 2001. **8**(3): p. 175-82.
81. Johnston, S.R.D., *New Strategies in Estrogen Receptor–Positive Breast Cancer.* American Association for Cancer Research, 2010. **16**(7): p. 1979-1987.
82. Zilli, M., et al., *Molecular mechanisms of endocrine resistance and their implication in the therapy of breast cancer.* Biochimica et Biophysica Acta (BBA) - Reviews on Cancer, 2009. **1795**(1): p. 62-81.
83. Hoogsteen, I.J., et al., *Expression of EGFR Under Tumor Hypoxia: Identification of a Subpopulation of Tumor Cells Responsible for Aggressiveness and Treatment Resistance.* International Journal of Radiation Oncology*Biology*Physics, 2012. **84**(3): p. 807-814.
84. Biscardi, J.S., et al., *c-Src-mediated Phosphorylation of the Epidermal Growth Factor Receptor on Tyr845 and Tyr1101 Is Associated with Modulation of Receptor Function.* Journal of Biological Chemistry, 1999. **274**(12): p. 8335-8343.